Title
NONLINEAR WAVE INTERACTION INVOLVING SURFACE POLARITONS

Authors
Shen, Y.R.
DeMartini, F.

Publication Date
1980-09-01

Lawrence Berkeley Laboratory
UNIVERSITY OF CALIFORNIA

Materials & Molecular Research Division

To be published as a chapter in Surface Polaritons, edited by V.M. Agranovitch and D.L. Mills, North-Holland Publishing Company, New York

NONLINEAR WAVE INTERACTION INVOLVING SURFACE POLARITONS

Y.R. Shen and F. DeMartini

September 1980

Prepared for the U.S. Department of Energy under Contract W-7405-ENG-48

DISCLAIMER

Surface Polaritons, edited by V. M. Agranovitch
and D. L. Mills

LBL-11358

NONLINEAR WAVE INTERACTION INVOLVING SURFACE POLARITONS

Y. R. Shen

Department of Physics
University of California
Berkeley, California 94720

Materials and Molecular Research Division
Lawrence Berkeley Laboratory
Berkeley, California 94720

and

F. DeMartini

Quantum Optics Laboratory
Istituto di Fisica, "G. Marconi"
Università di Roma
00185 Roma, Italy

I. Introduction

As a subarea of surface physics, surface polaritons have recently attracted much attention.[1] Linear optical properties of surface polaritons in various media have been extensively investigated. Their results and potential applications to surface and material studies are reviewed elsewhere in this book. Nonlinear optical studies involving surface polaritons are, however, very rare. From the physics point of view, the subject is actually a rather interesting one. First, since the surface polaritons are localized to a thin surface layer near an interface, nonlinear optical effects involving surface polaritons have a surface-specific nature. Then, surface nonlinear optics with all interacting waves being surface polaritons is possible, and forms a new branch in the field of nonlinear optics. With tunable laser excitations, surface nonlinear optical spectroscopy can be devised and applications can be envisioned. In this chapter, we shall review work in this area in the past few years. Emphasis will be on the experimental observation in comparison with theoretical prediction.

We shall begin with a theoretical discussion on wave interaction involving surface polaritons in Sec. II. The general theory of linear optical excitation of surface polaritons will first be given. It will then be extended to the case of nonlinear optical excitation with the nonlinear polarization as the driving source.[2] Actually, generation of surface polaritons by optical mixing of bulk waves can be considered as a special case of nonlinear optical reflection from a surface treated by Bloembergen and Pershan.[3] The general formalism can also be used to describe the generation of bulk and surface waves through mixing of sur-

face polaritons or surface polaritons with bulk waves.

The experimental demonstration of nonlinear excitations of surface polaritons will be reviewed in Sec. III. Two cases will be considered: one with GaP demonstrating nonlinear excitation of surface phonon-polaritons by difference-frequency mixing,[4] and the other with ZnO demonstrating second harmonic generation of surface exciton-polaritons.[5] It will then be shown that the surface polariton excitation can be probed through either mixing of the surface polaritons with a probe beam or surface roughness scattering. That nonlinear excitation of surface polaritons has some advantages over linear excitation and is useful for study of surface polaritons will also be discussed.

Second harmonic generation is the simplest nonlinear optical effect, and will be considered in Sec. IV to illustrate the interaction of surface polaritons. Here, surface plasmons will be the subject of discussion since they exist over a wide spectral range covering both the fundamental and the second harmonic. Nonlinearity in the case of a metal-air interface arises from the metal,[6] while in the case of a metal-dielectric interface may come mainly from the dielectric.[7] In the former case, a single atomic layer on the surface may be responsible for the observed nonlinearity.[8] Various aspects of the theory of Sec. II can be tested out by the experiments of second harmonic generation with surface plasmons.

Coherent antiStokes Raman scattering can also be carried out with surface plasmons.[9] This will be discussed in Sec. V. In general, four-wave mixing of surface plasmons should be observable, and can be used as a spectroscopic technique to probe resonances of a dielectric. The

technique has advantages over four-wave mixing spectroscopy in a bulk, and should be most useful for studying molecular overlayers and materials with strong absorption and fluorescence. With picosecond pulse excitation, the signal-to-noise ratio can be enhanced by orders of magnitude with a resulting sensitivity capable of detecting a submonolayer of adsorbed molecules.

Finally, in Sec. VI, we shall speculate on the future progress in the field. Applications to surface physics will be considered in particular. It seems likely that the combined force of surface nonlinear optics and surface physics may open up a new area of exciting interdisciplinary research.

II. Theory

A. Linear Excitation of Surface Polaritons

We consider here a general system of N layers shown in Fig. 1. The solution of plane wave propagation in such a medium is governed by the wave equation

$$[\nabla \times (\nabla x) - (\omega^2/c^2)\varepsilon(z)]\vec{E} = 0 \tag{1}$$

together with the boundary conditions. Assume that each layer is isotropic or cubic, and let the incoming wave be transverse magnetic

$$\vec{E}_o = (\hat{x}\, \&_{ox} + \hat{z}\, \&_{oz})e^{i(k_x x + k_{oz} z - \omega t)} \tag{2}$$

with $k_x \&_{ox} = - k_{oz} \&_{oz}$ and $k_o = (\omega/c)\sqrt{\varepsilon_o}$. Then, the reflected wave for

for $z < z_o$ is

$$\vec{E}_R = \left(\hat{x} + \hat{z}\,\frac{k_x}{k_{oz}}\right)\mathcal{E}_{Rx} e^{i(k_x x - k_{oz} z - \omega t)} . \qquad (3)$$

For $z_{j-1} < z < z_j$, the field is the sum of a transmitted wave and a reflected wave, and can be written as

$$\vec{E}_j = \{\hat{x}[A_j \cos k_{jz}(z - z_{j-1}) + B_j \sin k_{jz}(z - z_{j-1})]$$

$$+ \hat{z}\left(\frac{ik_x}{k_{jz}}\right)[- A_j \sin k_{jz}(z - z_{j-1}) + B_j \cos k_{jz}(z - z_{j-1})]\} e^{i(k_x x - \omega t)} \qquad (4)$$

with $k_j = (\omega/c)\sqrt{\varepsilon_j}$. Finally, for $z > z_N$, there is only an outgoing wave

$$\vec{E}_T = \left(\hat{x} - \hat{z}\,\frac{k_x}{k_{Tz}}\right)\mathcal{E}_{Tx} e^{i(k_x x + k_{Tz} z - \omega t)} . \qquad (5)$$

The 2N amplitude variables $\mathcal{E}_{Rx}$, ---, A_j, B_j, ---, and $\mathcal{E}_{Tx}$ are related by the boundary conditions.

$$\mathcal{E}_{Rx} - A_1 = - \mathcal{E}_{ox}$$

$$(\varepsilon_o k_x / k_{oz})\mathcal{E}_{Rx} - (i\varepsilon_1 k_x / k_{1z}) B_1 = (\varepsilon_o k_x / k_{oz})\mathcal{E}_{ox}$$

- -

$$(\cos k_{jz} d_j) A_j + (\sin k_{jz} d_j) B_j - A_{j+1} = 0$$

$$(i\varepsilon_j k_z / k_{jz})[- (\sin k_{jz} d_j) A_j + (\cos k_{jz} d_j) B_j] - (i\varepsilon_{j+1} k_x / k_{j+1,z}) B_{j+1} = 0$$

cont'd

- - - - - - - - - - - - - - - - - - - -

$$(\cos k_{Nz} d_N) A_N + (\sin k_{Nz} d_N) B_N - \mathcal{E}_{Tx} = 0$$

$$(i\varepsilon_N k_x / k_{Nz}) [- (\sin k_{Nz} d_N) A_N + (\cos k_{Nz} d_N) B_N] + (\varepsilon_T k_x / k_{Tz}) \mathcal{E}_{Tx} = 0 \qquad (6)$$

where $d_j = z_j - z_{j-1}$. The above set of equations can be written in the matrix form

$$\overleftrightarrow{D} \begin{pmatrix} \mathcal{E}_{Rx} \\ \vdots \\ A_j \\ B_j \\ \vdots \\ \mathcal{E}_{Tx} \end{pmatrix} = \begin{pmatrix} -\mathcal{E}_{ox} \\ \dfrac{\varepsilon_o k_x}{k_{oz}} \mathcal{E}_{ox} \\ 0 \\ \vdots \\ 0 \end{pmatrix} . \qquad (7)$$

Since $k_{jz} = [(\omega/c)^2 \varepsilon_j - k_x^2]^{1/2}$, so $\overleftrightarrow{D}$ is a function of k_x. In some cases, one may find that for $k_x = K_x$, the determinant $|\overleftrightarrow{D}(K_x)|$ vanishes. This actually means that the medium now has an electromagnetic resonance. In other words, in the absence of damping, an electromagnetic field would have generated with a vanishingly small input. If the resonant mode is a guided mode with field strength more or less confined to a particular layer interface, we call it a surface polariton. In general, a layered medium can have several such resonant modes.

We now consider the special case of a single film layer sandwiched between two semi-infinite media.

$$|\overleftrightarrow{D}| = \begin{vmatrix} -1 , & 1 , & 0 , & 0 \\ 1 , & 0 , & -iq_o/q_1 , & 0 \\ 0 , & \cosh_{1z}d_1 , & \sinh_{1z}d_1 , & -1 \\ 0 , & (-i/q_1)\sinh_{1z}d_1 , & (i/q_1)\cosh_{1z}d_1 , & 1/q_T \end{vmatrix}$$

$$= \frac{\cosh_{1z}d_1}{q_1^2 q_T} [i(q_1 q_o + q_1 q_T) + (q_1^2 + q_o q_T)\tanh_{1z}d_1] \tag{8}$$

where $q_j = k_{jz}/\varepsilon_j = [(\omega/c)^2\varepsilon_j - k_x^2]^{1/2}/\varepsilon_j$. For real ε_j, $|\vec{D}|$ will vanish only if k_{1z} is imaginary. Let $k_{1z} = -i\beta_1$. We find that for appropriate ε_j, we can have $|\vec{D}| = 0$, which is the dispersion relation of the surface polaritons

$$\tanh\beta_1 d_1 - \frac{q_1 q_o + q_1 q_T}{q_1^2 + q_o q_T} = 0. \tag{9}$$

If $\beta_1 d_1 \gg 1$, it reduces to

$$(q_1 - q_T)(q_1 - q_o) = 0 \tag{10}$$

or more explicitly in terms of $k_x = K_x$,

$$K_x^2 = \left(\frac{\omega}{c}\right)^2 \frac{\varepsilon_1 \varepsilon_T}{\varepsilon_1 + \varepsilon_T} \tag{11a}$$

$$K_x^2 = \left(\frac{\omega}{c}\right)^2 \frac{\varepsilon_1 \varepsilon_o}{\varepsilon_1 + \varepsilon_o} . \tag{11b}$$

These are the familiar dispersion relations for surface polaritons at an interface between two semi-infinite media.[10] Physically, $\beta_1 d_1 \gg 1$ cor-

responds to an optically thick film which effectively decouples the two interfaces so that the two surface polariton modes of Eqs. (11a) and (11b) are separately confined to the 0 - 1 and 1 - T interfaces respectively. Note that since k_{1z} is imaginary, Eq. (11a) (or (11b)) can be satisfied only if one of the two ε's in the equation is negative and the sum of the two ε's is also negative. Then, k_{zi} is imaginary and the field drops off exponentially on both sides of the interface. The surface polariton is physically confined to a thin layer of $(k_{z1}^{-1} + k_{zT}^{-1})$ thick at the interface and propagates with a wavevector K_x. In general, $\varepsilon = \varepsilon' + i\varepsilon''$ is complex for a medium, so that $K_x = K_x' + iK_x''$ with K_x' being the wavevector and K_x'' the attenuation constant for the surface polariton. Negative ε' arises in media with exciton or phonon reststrahlung bands or in metals below the plasma frequency.

Equation (6) or (7) determines the field amplitudes in the layered medium set up by the incoming wave of Eq. (2). When $k_x(\omega) \cong K_x'(\omega)$, the surface polariton is resonantly excited. For the case of a thin film sandwiched between two semi-infinite media, the solution of Eq. (6) or (7) is well known.[11]

$$
\begin{aligned}
\mathcal{E}_{Rx} &= \frac{r_{o1} + r_{1T}\exp(i2k_{1z}d_1)}{1 + r_{o1}r_{1T}\exp(i2k_{1z}d_1)}\,\mathcal{E}_{ox} \\
\mathcal{E}_{Tx} &= \frac{t_{o1}t_{1T}\exp(ik_{1z}d_1)}{1 + r_{o1}r_{1T}\exp(i2k_{1z}d_1)}\left(\frac{k_{Tz}^2\varepsilon_o}{k_{oz}^2\varepsilon_T}\right)\mathcal{E}_{ox} \\
A_1 &= \frac{(1 + r_{o1})[1 + r_{1T}\exp(i2k_{1z}d_1)]}{1 + r_{o1}r_{1T}\exp(i2k_{1z}d_1)}\,\mathcal{E}_{ox} \\
B_1 &= \frac{(1 - r_{o1})[1 - r_{1T}\exp(i2k_{1z}d_1)]}{1 + r_{o1}r_{1T}\exp(i2k_{1z}d_1)}\left(\frac{i\varepsilon_o k_{1z}}{\varepsilon_1 k_{oz}}\right)\mathcal{E}_{ox}
\end{aligned}
\qquad (12)
$$

where r_{o1}, r_{1T}, T_{o1}, and t_{1T} are the Fresnel coefficients.

$$r_{ij} = \frac{\varepsilon_j k_{iz} - \varepsilon_i k_{jz}}{\varepsilon_j k_{iz} + \varepsilon_i k_{jz}}$$

$$t_{ij} = \frac{2\sqrt{\varepsilon_i \varepsilon_j}\, k_{iz}}{\varepsilon_j k_{iz} + \varepsilon_i k_{jz}} . \tag{13}$$

It is easy to show that $|D| \propto [1 + r_{o1} r_{1T} \exp(i2k_{1z}d_1)]$ and hence the relation

$$1 + r_{o1} r_{1T} \exp(i2k_{1z}d_1) = 0 \tag{14}$$

is equivalent to Eq. (9) representing the dispersion relation of surface polaritons.

In practice, two kinds of geometry are often used to linearly excite surface polaritons in the above sandwich medium. They are shown in Fig. 2. For the Otto configuration of Fig. 2a,[12] we have $\varepsilon'_T < 0$ and $\varepsilon'_o > \varepsilon'_1 > 0$. The surface polariton that is excited when $k_x(\omega) \cong K'_x(\omega)$ is more or less confined to the 1 - T interface. For the Kretschmann configuration of Fig. 2b,[13] we have $\varepsilon'_1 < 0$ and $\varepsilon'_o > \varepsilon'_T > 0$. The surface polariton excited is again more or less confined to the 1 - T interface. In this latter case, there may also exist a surface polariton mode confined to the 0 - 1 interface, but since $K'_x > |k_o|, |k_T|$, it cannot be linearly excited by the prism coupler in Fig. 2. In both cases, when the surface polariton is excited, a reflectivity dip should be observed according to Eq. (12). With optimum choice of the film thickness d_1, the reflectivity dip can reach a minimum close to 0. An example is

shown in Fig. 3.

Excitation of surface polaritons is basically the same as excitation of guided optical waves. Thus, instead of prism coupling, a grating on the surface can also be used as the coupler for linear excitation of surface polaritons. Here, the phase mismatch between k_x and K'_x is compensated by the reciprocal lattice vector of the periodic grating in the resonant excitation. Then, surface roughness can also be effective as a coupler for surface polariton excitation since it can be considered as a random grating.

B. Nonlinear Excitation of Surface Polaritons

Surface polaritons can also be excited through nonlinear optical mixing in the medium.[2] The basic idea is fairly simple. Nonlinear mixing induces a nonlinear polarization $\vec{P}^{NL}(\omega,\vec{k}_s) = \vec{\mathcal{P}}^{NL} e^{i(\vec{k}_s \cdot \vec{r} - \omega t)}$ in the medium, which, being a collection of oscillating dipoles, acts as a source for generation of the field at ω. If $k_{sx} \cong K'_x(\omega)$, then the surface polariton is resonantly excited. Mathematically, we can treat the problem as an extension of the derivation given in the previous section for linear excitation. First, the wave equation becomes

$$[\nabla \times (\nabla x) - (\omega^2/c^2)\epsilon(z)]\vec{E} = (4\pi\omega^2/c^2)\vec{P}^{NL}(\omega,\vec{k}_s). \qquad (15)$$

Then, the field is obtained as a sum of homogeneous and particular solutions. Assume $\vec{E}_o = 0$. For $z < z_o$

$$\vec{E}_R = (\hat{x} + \hat{z}\, k_x/k_{oz})\mathcal{E}_{Rx} e^{i[k_x x - k_{oz}(z-z_o) - \omega t]} \qquad \text{cont'd}$$

$$+ [\hat{x}(\gamma^{o}_{xx}\mathcal{P}^{NL}_{ox} + \gamma^{o}_{xz}\mathcal{P}^{NL}_{oz}) + \hat{z}(\gamma^{o}_{zx}\mathcal{P}^{NL}_{ox} + \gamma^{o}_{zz}\mathcal{P}^{NL}_{oz})]e^{i[k_{sox}x+k_{soz}(z-z_o)-\omega t]} . \tag{16a}$$

For $z_{j-1} < z < z_j$,

$$\vec{E}_j = \{\hat{x}[A_j \cos k_{jz}(z - z_{j-1}) + B_j \sin k_{jz}(z - z_{j-1})]$$

$$+ \hat{z}(ik_x/k_z)[- A_j \sin k_{jz}(z - z_{j-1}) + B_j \cos k_{jz}(z - z_{j-1})]\}e^{i(k_x x-\omega t)}$$

$$+ [\hat{x}(\gamma^{j}_{xx}\mathcal{P}^{NL}_{jx} + \gamma^{j}_{xz}\mathcal{P}^{NL}_{jz}) + \hat{z}(\gamma^{j}_{zx}\mathcal{P}^{NL}_{jz} + \gamma^{j}_{zz}\mathcal{P}^{NL}_{jz})]e^{i[k_{sjz}x+k_{sjz}(z-z_{j-1})-\omega t]} . \tag{16b}$$

For $z > z_N$

$$\vec{E}_T = (\hat{x} - \hat{z}\, k_x/k_{Tz})\mathcal{E}_{Tx}e^{i[k_x x+k_{Tz}(z-z_N)-\omega t]}$$

$$+ [\hat{x}(\gamma^{T}_{xx}\mathcal{P}^{NL}_{Tx} + \gamma^{T}_{xz}\mathcal{P}^{NL}_{Tz}) + \hat{z}(\gamma^{T}_{zx}\mathcal{P}^{NL}_{Tx} + \gamma^{T}_{zz}\mathcal{P}^{NL}_{Tz})]e^{i[k_{sTx}x+k_{sTz}(z-z_N)-\omega t]} . \tag{16c}$$

In Eq. (16), the $\mathcal{P}^{NL}$ terms are the particular solutions in various regions obtained from Eq. (15). The boundary conditions require that $k_{sRx} = k_{sjx} = k_{sTx} = k_x$, and

$$\overleftrightarrow{D}\begin{pmatrix} \mathcal{E}_{Rx} \\ \vdots \\ A_j \\ B_j \\ \vdots \\ \mathcal{E}_{Tx} \end{pmatrix} = \begin{pmatrix} -\left(\gamma^{o}_{xx}\mathcal{P}^{NL}_{ox} + \gamma^{o}_{xz}\mathcal{P}^{NL}_{oz}\right) + \left(\gamma^{1}_{zx}\mathcal{P}^{NL}_{1x} + \gamma^{1}_{zz}\mathcal{P}^{NL}_{1z}\right) \\ \vdots \\ -\left(\gamma^{j}_{xx}\mathcal{P}^{NL}_{jx} + \gamma^{j}_{xz}\mathcal{P}^{NL}_{jz}\right)\exp(ik_{sjz}d) + \left(\gamma^{j+1}_{zx}\mathcal{P}^{NL}_{j+1,x} + \gamma^{j+1}_{zz}\mathcal{P}^{NL}_{j+1,z}\right) \\ -\varepsilon_j\left[\gamma^{j}_{zx}\mathcal{P}^{NL}_{jx} + \left(\gamma^{j}_{zz} + \frac{4\pi}{\varepsilon_j}\right)\mathcal{P}^{NL}_{jz}\right]\exp(ik_{sjz}d) + \varepsilon_{j+1}\left[\gamma^{j+1}_{zx}\mathcal{P}^{NL}_{j+1,x} + \left(\gamma^{j+1}_{zz} + \frac{4\pi}{\varepsilon_{j+1}}\right) \times \mathcal{P}^{NL}_{j+1,z}\right] \\ \vdots \\ -\varepsilon_N\left[\gamma^{N}_{zx}\mathcal{P}^{NL}_{Nx} + \left(\gamma^{N}_{zz} + \frac{4\pi}{\varepsilon_N}\right)\mathcal{P}^{NL}_{Nz}\right]\exp(ik_{sNz}d) + \varepsilon_T\left[\gamma^{T}_{zx}\mathcal{P}^{NL}_{Tx} + \left(\gamma^{T}_{zz} + \frac{4\pi}{\varepsilon_T}\mathcal{P}^{NL}_{Tz}\right)\right] \end{pmatrix}. \tag{17}$$

In comparison with Eq. (7) for linear excitation, the nonlinear polarization $\mathcal{P}^{NL}$ here plays the role of the incoming field $\mathcal{E}_o$ in the linear case. Again, as $k_{sx} \equiv k_x \cong K'_x(\omega)$, the surface polariton is excited.

An important difference between linear and nonlinear excitations should however be noted. In the linear case, it is not possible to excite a surface polariton on a smooth interface between two semi-infinite media because the wavevector $k(\omega)$ of the incoming exciting wave in either medium is always smaller than $K'_x(\omega)$. In the nonlinear case, this becomes possible because optical mixing induces a nonlinear polarization with a wavevector $\vec{k}_s$ which is the vector sum of the wavevectors of the exciting fields, and in general, one can have $k_{sx} = K'_x$. Here, Eq. (17) reduces to

$$\overleftrightarrow{D}\begin{pmatrix} \mathcal{E}_{Rx} \\ \mathcal{E}_{Tx} \end{pmatrix} = \begin{pmatrix} -\left(\gamma^{o}_{xx}\mathcal{P}^{NL}_{ox} + \gamma^{o}_{xz}\mathcal{P}^{NL}_{oz}\right) + \left(\gamma^{T}_{zx}\mathcal{P}^{NL}_{Tx} + \gamma^{T}_{zz}\mathcal{P}^{NL}_{Tz}\right) \\ -\varepsilon_o\left[\gamma^{o}_{zx}\mathcal{P}^{NL}_{ox} + \left(\gamma^{o}_{zz}\mathcal{P}^{NL}_{oz} + \frac{4\pi}{\varepsilon_o}\right)\right] + \varepsilon_T\left[\gamma^{T}_{zx}\mathcal{P}^{NL}_{TX} + \left(\gamma^{T}_{zz}\mathcal{P}^{NL}_{Tz} + \frac{4\pi}{\varepsilon_T}\right)\right] \end{pmatrix}. \tag{18}$$

with

$$\overleftrightarrow{D} = \begin{pmatrix} 1 & , & -1 \\ \dfrac{\varepsilon_o k_x}{k_{oz}} & , & \dfrac{\varepsilon_T k_x}{k_{Tz}} \end{pmatrix}$$

$$|\overleftrightarrow{D}| = (\varepsilon_o k_{Tz} + \varepsilon_T k_{oz})/k_{oz}k_{Tz}$$

$$= \frac{(\varepsilon_T - \varepsilon_o)}{k_{oz}k_{Tz}(\varepsilon_o k_{Tz} - \varepsilon_T k_{oz})} \left[(\varepsilon_T + \varepsilon_o)K_x^2 - \frac{\omega^2}{c^2}\varepsilon_T\varepsilon_o\right]. \qquad (19)$$

Again, $|\overleftrightarrow{D}| = 0$ yields the familiar surface polariton dispersion relation

$$K_x^2 = (\omega^2/c^2)\varepsilon_T\varepsilon_o/(\varepsilon_T + \varepsilon_o).$$

As an example, we consider the special case where $\vec{P}_o^{NL} \neq 0$ but $\vec{P}_T^{NL} = 0$.[2] The particular solution of Eq. (15) gives

$$\gamma_{xx}^o = 4\pi k_{oz}^2/\varepsilon_o(k_{os}^2 - k_o^2)$$

$$\gamma_{xz}^o = -4\pi k_x k_{osz}/\varepsilon_o(k_{os}^2 - k_o^2)$$

$$\gamma_{zx}^o = -4\pi k_x k_{osz}/\varepsilon_o(k_{os}^2 - k_o^2)$$

$$\gamma_{zz}^o = -4\pi(k_{osz}^2 - k_o^2)/\varepsilon_o(k_{os}^2 - k_o^2). \qquad (20)$$

Then, the solution of Eq. (18) yields

$$\mathscr{E}_{Rx} = \frac{4\pi\varepsilon_T k_{oz}}{\varepsilon_o(\varepsilon_o k_{Tz} + \varepsilon_T k_{oz})(k_{os}^2 - k_o^2)}$$

$$\left[\mathscr{P}_{ox}^{NL}(k_{os}^2 - k_o^2) + \left(\frac{\varepsilon_o}{\varepsilon_T} k_{Tz} - k_{osz}\right)(k_{osz}\mathscr{P}_{ox}^{NL} - k_x\mathscr{P}_{oz}^{NL})\right]$$

$$\mathscr{E}_{Tx} = \frac{-4\pi k_{Tz}}{(\varepsilon_o k_{Tz} + \varepsilon_T k_{oz})(k_{os}^2 - k_o^2)}$$

$$[\mathscr{P}_{ox}^{NL}(k_{os}^2 - k_o^2) - (k_{oz} + k_{osz})(k_{osz}\mathscr{P}_{ox}^{NL} - k_x\mathscr{P}_{oz}^{NL})]. \qquad (21)$$

When $k_x = K_x'$, the real part of $(\varepsilon_o k_{Tz} - \varepsilon_T k_{oz})$ vanishes, and hence $\mathscr{E}_R$ and $\mathscr{E}_T$ are resonantly enhanced. The excited surface polariton actually corresponds to only the homogeneous part of Eq. (16), i.e.,

$$\vec{E}_{SP} = (\hat{x} + \hat{z}\, k_x/k_{oz})\mathscr{E}_{Rx} e^{i(k_x x - \omega t) + \beta_o z} \quad \text{for } z < 0$$

$$= (\hat{x} + \hat{z}\, k_x/k_{Tz})\mathscr{E}_{Tx} e^{i(k_x x - \omega t) - \beta_T z} \quad \text{for } z > 0 \qquad (22)$$

where $\beta_o = -i\, k_{oz}$ and $\beta_T = -i\, k_{Tz}$.

The surface polariton described here by Eq. (22) is a driven wave. In general, there should also exist at the interface free surface polariton waves which are solution of $\overleftrightarrow{D}\begin{pmatrix}\mathscr{E}_{Rx}\\ \mathscr{E}_{Tx}\end{pmatrix} = 0$. As in the bulk case, the amplitude of the free wave is determined by matching the boundary conditions on the interface. For infinite plane wave excitation, the free wave vanishes. For excitation over a finite cross-section, on the other hand, the free wave can be important; in particular, it may be the only wave present in regions with no excitation. However, if excitation over

a finite cross-section can be Fourier decomposed into a set of infinite plane waves, then there is no need to include the free wave in the solution again.

C. Nonlinear Interaction of Surface Polaritons

As electromagnetic waves, surface polaritons can also interact nonlinearly. In fact, with linear pulsed laser excitation, the surface polariton intensity being confined to a thin layer can reach unusally high value. The nonlinear polarization induced by mixing of surface polaritons is correspondingly large. Thus, even though $\vec{P}^{NL}$ is nonvanishing only in a very thin layer near the interface, the field generated may be readily observable. That $\vec{P}^{NL}$ can be greatly enhanced through enhancement of pump field intensities via surface polariton excitations makes the study of nonlinear optical effects on surfaces very appealing.

The output field of surface polariton mixing is again governed by the wave equation in Eq. (15). Actually, the general solution of Eq. (15) discussed in the previous section is still valid. Consider the case where the surface polaritons can be well approximated as being confined to a single interface at z = 0. Then, $\vec{P}^{NL}(\omega,\vec{k}_s)$ can be written as

$$\vec{P}^{NL}(\omega,\vec{k}_s) = \vec{\mathscr{P}}_o^{NL} e^{i(k_{sx}s-\omega t)+\sigma_o z} \quad \text{for } z < 0$$

$$= \vec{\mathscr{P}}_T^{NL} e^{i(k_{sx}x-\omega t)-\sigma_T z} \quad \text{for } z > 0. \qquad (23)$$

If $k'_{sx} \cong K'_x(\omega)$, the surface polariton at ω can again be resonantly excited by $\vec{P}^{NL}(\omega,\vec{k}_s)$. This corresponds to a phase-matched generation of

surface polariton by mixing of surface polaritons. With all waves involved being surface waves, we have here a true surface nonlinear optical effect. The wavevector component k'_{sx} can also be less than the bulk wavevector k_o (or/and k_T). In this case, the output is a bulk wave with its direction of propagation defined by the exit angle $\theta = \sin^{-1}(k_{sx}/k_o)$ with respect to the surface normal.

More generally, one can consider the problem of optical mixing of surface polaritons with bulk waves. Since some of the pump fields are surface waves, $\vec{P}^{NL}(\omega,\vec{k}_s)$ induced is again confined to a thin layer near the interface. Equation (15) and its solution discussed in the previous section are clearly also applicable to such a problem. The output can be either surface polariton wave or bulk wave depending on the value of k_{sx}.

III. Nonlinear Excitation of Surface Polaritons — Experimental Demonstration

That surface polaritons can be excited by nonlinear optical mixing has been demonstrated on semiconductor surfaces.[4,5] In semiconductors, two types of polariton reststrahlung bands may appear: phonon-polariton and exciton polariton. The dielectric constant in the reststrahlung band may become more negative than -1, and hence, according to Eq. (11), surface polaritons can exist, at least at the air-semiconductor interface. Many semiconductors possess large second-order optical nonlinearity. It is then possible to induce a second-order nonlinear polarization $\vec{P}^{(2)}(\omega, \vec{k}_s)$ in a semiconductor by sum- or difference-frequency mixing. If $k_{sx} \cong K'_x(\omega)$, the surface polariton will be excited.

We consider first the nonlinear excitation of surface phonon-polari-

tons at the air-GaP (110) interface.[4] The infrared dielectric constant of GaP in the frequency region around the 367-cm^{-1} transverse phonon mode is[14]

$$\epsilon(\omega) = \epsilon_\infty + \omega_p^2/(\omega_T^2 - \omega^2 - i\omega_T\Gamma) \tag{24}$$

with $\epsilon_\infty = 9.091$, $\omega_T = 367.3\ cm^{-1}$, $\omega_p^2 = 1.859\ \omega_T^2$, and $\Gamma = 1.28\ cm^{-1}$. In a narrow region with $\omega > \omega_T$, we find $\epsilon(\omega) < -1$. Surface polaritons can then exist with a dispersion relation

$$(K_x' + i\ K_x'')^2 = (\omega/c)^2\epsilon/(1 + \epsilon) \tag{25}$$

plotted in Fig. 4. To demonstrate the nonlinear excitation of surface polaritons on GaP, we used the experimental setup shown in Fig. 5. A Q-switched ruby laser provided the ω_1 beam at 14403 cm^{-1}. It was then also used to pump two dye laser systems to provide beams at ω_2 and ω_3. In the experiment, ω_3 was fixed at 13333 cm^{-1} while ω_2 was tuned between 14006 and 14035 cm^{-1}. The ω_1 and ω_2 beams were used to excite surface polaritons, and the ω_3 beam to probe the excited surface polaritons

Let $\hat{\bar{x}}$, $\hat{\bar{y}}$, and $\hat{\bar{z}}$ be the crystal axes along [100], with $\hat{\bar{z}} \parallel \hat{y}$ and $\hat{\bar{x}}$ and $\hat{\bar{y}}$ at 45° with respect to the surface normal $\hat{z}$. We polarized the incoming fields at ω_1 and ω_2 as $\vec{E} = \hat{\bar{z}}\ E_1$, and $E_2 \approx \hat{x}\ \vec{E}_2 = (\hat{\bar{x}} + \hat{\bar{y}})E_2/\sqrt{2}$. Then, the induced nonlinear polarization in GaP was

$$\vec{P}_o^{NL}(\omega,\vec{k}_s) \cong \chi_{14}^{(2)}(\omega = \omega_1 - \omega_2)\hat{x}\ E_1E_2^* \tag{26}$$

with $\vec{k}_s = \vec{k}_1 - \vec{k}_2$. By adjusting the angle between ω_1 and ω_2 beams, k_{sx} could be varied from 0 to nearly $(k_1 + k_2)$. In our experiment, $\omega = \omega_1 - \omega_2$ was fixed in the range between 368 and 397 cm^{-1} where surface polaritons can exist, and k_{sx} was then varied around $k_{sx} \cong K'_x(\omega)$. It is, of course, also possible to fix k_{sx} and scan $\omega = \omega_1 - \omega_2$ to make $k_{sx} \cong K'_x(\omega)$ for surface polariton excitation. The generated surface polariton field should have the form of E_{SP} described in Eqs. (22) and (21) with the subindices 0 and T referring to GaP and air respectively, $\vec{P}^{NL}_{oz} \cong 0$, $\varepsilon_T = 1$, and $(\varepsilon_o k_{Tz} + k_{oz}) \propto (-k_x + K'_x + i\, K''_x)$. We find

$$\mathcal{E}_{Rx} = \frac{A}{-\Delta k_x + i\, K''_x} \mathcal{P}^{NL}_{ox}$$

$$\mathcal{E}_{Tx} = [k_{Tz}(k_{osz}k_{oz} + k^2_{oz})/k_{oz}(k_{osz}k_{Tz} - k^2_{oz}/\varepsilon_o)]\mathcal{E}_{Rx} \qquad (27)$$

where

$$A = -[2\pi(k_{oz} - \varepsilon_o k_{Tz})/K'_x\varepsilon_o(1 - \varepsilon^2_o)(k^2_{os} - k^2_o)](\varepsilon_o k_{osz}k_{Tz} - k^2_{oz})$$

$$\Delta k_x = k_x - K'_x.$$

It is seen that the generated surface polariton intensity ($\propto |E_{SP}|^2$) as a function of the phase mismatch Δk_x is a Lorentzian.

To demonstrate the presence of the generated surface polariton, we used the ω_3 beam as a probe with $\vec{E}_3$ along $\hat{z} \parallel \hat{y}$. Optical mixing of the probe beam with the surface polaritons in GaP also induced a second-order nonlinear polarization

$$\vec{P}_o^{NL}(\omega_4) = \chi_{14}^{(2)}(\omega_4 = \omega_3 - \omega)[\hat{x}\,\mathcal{E}_{Rz}^{*} + \hat{z}\,\mathcal{E}_{Rx}^{*}]\mathcal{E}_3$$

$$\times \exp[i(k_{3x} - k_x)x + (i\,k_{3z} - \beta_o)z - \omega_4 t] \qquad (28)$$

where $\vec{k}_3$ is the wavevector of the probe beam in GaP. As expected from Eq. (28), the output generated by $\vec{P}^{NL}(\omega_4)$ should have TM polarization and should be coherent with its direction fixed by the phase matching relation $k_{1x} - k_{2x} = k_{3x} - k_{4x}$ or equivalently $\vec{k}_4 = \vec{k}_3 - (\vec{k}_1 - \vec{k}_2)$. This was actually observed in the experiment. The output intensity can be estimated from the general solution for $\vec{E}(\omega_4)$ in Eqs. (16a), (16c), and (21), and should be proportional to $|\vec{P}_o^{NL}(\omega_4)|^2$.

$$I(\omega_4,\Delta k_x) \propto |\vec{P}_o^{NL}(\omega_4)|^2 = |\overleftrightarrow{\chi}^{(2)}(\omega_4 = \omega_3 - \omega):\vec{E}(\omega_3)\vec{E}_{SP}(\omega)|^2$$

$$\propto \frac{1}{\Delta k_x^2 + K_x''^2}\,|\chi_{14}^{(2)}(\omega_4 = \omega_3 - \omega)\chi_{14}^{(2)}(\omega = \omega_1 - \omega_2)^{*}E_1^{*}E_2E_3|^2. \qquad (29)$$

This explicitly shows that the output signal versus Δk_x should be a Lorentzian with its peak at $\Delta k_x = k_x - K_x'(\omega) = 0$ and its half width equal to K_x''. The experimental results could indeed be fit by Eq. (29). Typical examples are given in Fig. 6. From the observed half widths of $I(\omega_4,\Delta k_x)$ at various ω, we deduced $K_x'(\omega)$ and $K_x''(\omega)$, as is presented in Fig. 4. They are in good agreement with the theoretical curves calculated from the dispersion relation of Eq. (25). The attenuation coefficient $K_x''(\omega)$ is more sensitive to the frequency dependence of $\varepsilon(\omega)$ than $K_x'(\omega)$. The dashed curves in Fig. 4 were calculated with $\varepsilon(\omega)$ derived from a multi-

oscillator model of Barker[15] instead of the single-oscillator model used in Eq. (24). The experimental results seem to agree better with the multi-oscillator model. Towards small K_x'', the measured half width of $I(\omega_4, \Delta k_x)$ in Fig. 4 appears to have a limiting value. This was because when K_x'' was very small, the observed width was dominated by the finite spread of $\vec{k}$ of the laser beams. With a 50-KW peak power in each of the three laser beams, the peak output was about 0.1 μW at ω = 380 cm^{-1}, compared to a theoretical prediction of 0.27 μW.

Nonlinear optical excitation of surface exciton-polaritons has also been demonstrated using ZnO.[5] In this case, because excitons only exist at low temperatures, surface exciton-polaritons also exist only at low temperatures. In fact, this makes the linear excitation of surface exciton-polaritons rather difficult[16] since the Otto method with critical adjustment of prism spacing from the surface required for optical coupling is not easy to carry out in a helim cryostat. Nonlinear excitation by optical mixing, however, bypasses such difficulty.

ZnO is a uniaxial crystal. It has three prominent excitons, A, B, and C, near the band edge. We consider here only surface polaritons associated with the C-exiton. Because of anisotropy of ZnO, the surface polariton dispersion relation for the ZnO-air (or liquid helium) interface in the C-exciton reststrahlung band between 3.421 and 3.427 eV is somewhat different from Eq. (11) and is given by[17]

$$K_x^2 = \left(\frac{\omega}{c}\right)^2 \frac{\varepsilon_T \varepsilon_{ox}(\varepsilon_{ox} - \varepsilon_T)}{\varepsilon_{ox}\varepsilon_{oz} - \varepsilon_T^2} \tag{30}$$

with $\varepsilon_{bx} < 0$ and $\varepsilon_{bz} > \varepsilon_T$ or $\varepsilon_{bz} < 0$. If the ZnO crystal is oriented

with its c-axis in the surface along $\hat{x}$, then since the electric dipole transition for the C-exiton is only allowed for polarization parallel to the c-axis, we have, in the reststrahlung band of the exciton,

$$\varepsilon_{ox} = \varepsilon_{\infty} - \frac{(\varepsilon_{oo} - \varepsilon_{\infty})\omega_T^2}{(\omega^2 - \omega_T^2) + i\omega\Gamma}$$

$$\varepsilon_{oz} = \varepsilon_{\infty} \tag{31}$$

following the single-oscillator model and neglecting the anisotropy in ε_{∞}, where ω_T is the transverse exciton frequency, Γ is the damping constant, and $(\varepsilon_{oo} - \varepsilon_{\infty})$ is proportional to the exciton oscillator strength. By fitting the experimental dispersion curve with Eqs. (30) and (31), the constants ε_{∞}, ε_o, ω_T, and Γ can be determined.

The surface exciton-polariton here can be excited by sum-frequency mixing, or more simply, by second-harmonic generation.[5] The actual experimental setup used for the observation was shown in Fig. 7, and was much simpler than that for the case of GaP. The sample was immersed in superfluid helium. To excite the surface polariton at ω, the dye laser frequency was fixed at $\omega_1 = \frac{1}{2}\omega$, and the beam direction was varied to vary $k_x = 2k_{1x}$ around $K_x'(\omega)$. The excited surface polariton could again be probed through mixing with a probe beam. However, in the present case, since uv photons can be easily detected, the excited surface polaritons could be observed through surface roughness scattering even though the scattering efficiency is usually small for relatively smooth surfaces. Therefore, as shown in Fig. 7, the excitation of surface polaritons was monitored simply by a single photomultiplier.

In the experiment, incoming wave of either TE or TM was used. In the former case, the induced second-order nonlinear polarization in ZnO had only an $\hat{x}$ component

$$P_x^{NL}(\omega) = \chi_{31}^{(2)} E_y^2(\omega_1). \tag{32}$$

In the latter case, the $\hat{x}$-component of $\vec{P}^{NL}(\omega)$ dominated

$$P_x^{NL}(\omega) = \chi_{31}^{(2)} E_z^2(\omega_1) + \chi_{33}^{(2)} E_x^2(\omega_1). \tag{33}$$

The surface polariton field generated by $\vec{P}_x^{NL}(\omega)$ can again be calculated from Eqs. (22) and (21). For a 30-nsec input pulse with 50 KW peak power focused to a $\sim$ 50 μm spot, the surface polariton intensity should correspond to 10^8 photons/pulse. Experimentally, 10^4 photons/pulse was observed, suggesting that the surface roughness coupling efficiency was about 10^{-4}.

As in the case of GaP, the surface polariton intensity $I(\omega)$ versus $\Delta k_x = k_x - K_x'(\omega)$ should be a Lorentzian. This is seen by the fit to the experimental data in Fig. 8. The values of $K_x'(\omega)$ and $K_x''(\omega)$ deduced from the fit is plotted in Fig. 9. A least square fitting of these data points with Eqs. (30) and (31) yielded $\varepsilon_\infty = 6.15 \pm 0.01$, $\omega_T = 3.421$ eV, $\varepsilon_o = 6.172 \pm 0.01$, and $\Gamma = 0.25 \pm 0.05$ meV. They can be compared with the following values reported in the literature. $\varepsilon_\infty = 6.15$, $\omega_T = 3.4213$ eV, $\varepsilon_o = 6.188$, and $\Gamma = 0.5$ meV.

It is interesting to note that although the data in Fig. 8 appear to be quite scattered, the accuracy of determining $K_x'(\omega)$ from the results

is excellent. This is because the uncertainty is only $\pm K_x''$, and here $K_x''/K_x' \sim 10^{-2}$. Excitons in the uv are known to be fairly critically dependent of the surface condition. With nonlinear excitation, surface exciton-polaritons can be studied without further surface perturbation aside from original sample preparation. This is a clear advantage over the linear excitation method. Then, the nonlinear excitation method can, in principle, also be used to study surface exciton-polaritons under specific surface perturbation.

Unlike linear excitation, the nonlinear excitation method has the advantage that it can be used to excite and study surface polaritons at the interface of two semi-infinite media. Of course, the same method can also be used to study surface polaritons in layered media. In fact, with nonlinear excitation, it may even be possible to excite surface polaritons at an inner interface that cannot be reached by linear excitation.

IV. Second Harmonic Generation by Surface Plasmons

The dielectric constant of a metal is negative below the plasma frequency. Surface polaritons can therefore exist at a metal-dielectric interface. They are usually called surface plasmons.[1] If the dielectric medium is anisotropic, the surface plasmon dispersion relation is given by

$$K_x^2(\omega) = \left(\frac{\omega}{c}\right)^2 \frac{\varepsilon_m \varepsilon_\perp (\varepsilon_\parallel - \varepsilon_m)}{\varepsilon_\perp \varepsilon_\parallel - \varepsilon_m^2} \tag{34}$$

where $\varepsilon_m < 0$ is the dielectric constant of the metal with $\varepsilon_m^2 > \varepsilon_\perp \varepsilon_\parallel$, and

$\varepsilon_\perp > 0$ and $\varepsilon_\parallel > 0$ are respectively the dielectric constants of the dielectric medium perpendicular and parallel to the propagation direction of the surface plasmon. If the dielectric medium is isotropic, Eq. (34) reduces to

$$K_x^2(\omega) = \left(\frac{\omega}{c}\right)^2 \frac{\varepsilon_m \varepsilon}{\varepsilon_m + \varepsilon} . \tag{35}$$

Usually, the Kretschmann method of Fig. 2b is used to excite surface plasmons. The metal medium is simply a film of a few hundred Å sandwiched between the prism and the dielectric. The surface plasmon excited is confined more or less to the metal-dielectric interface. Its dispersion is somewhat different from that for two semi-infinite media, and in the case of isotropic dielectric, is given by Eq. (9). However, since the metal film can be regarded as optically thick, Eq. (34) or (35) is actually a very good approximation of the true dispersion.

With an appropriately chosen metal film thickness in the Kretschmann geometry, the surface plasmon can be optimally excited. A sizable fraction of the exciting beam power is coupled into the surface plasmon, and hence the surface plasmon intensity is greatly enhanced in comparison with the incoming beam intensity. For example, the enhancement observed in practice can be $\sim$ 400 for a silver-air interface and $\sim$ 100 for a silver-dielectric ($\varepsilon \sim 2.5$) interface. The strongly enhanced intensity facilitates the study of nonlinear optical processes at the interface.

The simplest nonlinear optical process is the second harmonic generation. It was first demonstrated by Simon and coworkers at the silver-air interface.[6] The theoretical treatment of the problem follows the

general formalism in Sec. II. First, the fundamental surface plasmon field obtained from linear excitation is calculated. Then, the second harmonic output is obtained from the solution of the wave equation discussed in Sec. II with an induced nonlinear polarization $\vec{P}^{NL}(\omega = 2\omega_1)$ in the silver metal as the driving source. Since metal has inversion symmetry, $\vec{P}^{NL}(\omega)$ arises only through electric quadrupole and magnetic dipole contribution and is relatively weak.[8] From symmetry consideration, it can be written as[8]

$$\vec{P}^{NL}(\omega = 2\omega_1) = \alpha(\vec{E}_1 \cdot \nabla)\vec{E}_1 + \beta(\nabla \cdot \vec{E}_1)\vec{E}_1 + \gamma\vec{E}_1 \times \vec{B}_1 \qquad (36)$$

where α, β, and γ are constant coefficients. The first two terms are of electric-quadrupole origin. Since they depend on spatial variation of the fundamental field $\vec{E}_1$, in uniform metallic media, they are only nonvanishing near the surface within the Thomas-Fermi screening length, i. e., within one or two atomic layers thick. In fact, they can be regarded as arising from electric-dipole nonlinearity of the surface atomic layers that do not have inversion symmetry. The last term of Eq. (36) is of magnetic dipole origin, and is nonvanishing throughout the bulk. However, it is usually negligible compared with the electric quadrupole terms. A single layer of atoms without inversion symmetry already has a second-order nonlinearity much larger than that of the magnetic-dipole contribution from a hundred atom layers penetrated by the exciting field, as evidenced by the investigation of Bloembergen et al.[8]

Even though the nonlinearity is rather weak, second harmonic generation by surface plasmons at the metal-air interface is readily observ-

able with the setup in Fig. 10.[6] The results generally follow the theoretical predictions of Sec. II. In particular, for copropagating fundamental surface plasmons, the second harmonic output is a coherent beam with its propagation direction specified by $2k_{1x}$ along the surface and its polarization being transverse magnetic. For counter-propagating fundamental surface plasmons, $\vec{P}^{NL}(\omega)$ has a zero wavevector component along the surface. The second harmonic output should then be propagating along the normal of the surface.[18] From symmetry, however, the component of $\vec{P}^{NL}(\omega)$ of Eq. (36) perpendicular to the surface normal is zero, and hence, no output can be observed.[19] By varying the angle between the two propagating surface plasmons, the coefficients α, β, and γ in Eq. (36) can in principle be determined from the observed second harmonic signals.

The second harmonic output can be greatly enhanced if air is replaced by a nonlinear crystal in the above case.[7] The nonlinearity is now dominated by the crystal instead of the metal. For a quartz-metal interface, for example, the nonlinear susceptibility $\chi^{(2)}$ for quartz is one order of magnitude larger than the effective $\chi^{(2)}$ for metal, so that the output is two orders of magnitude stronger. Then, the symmetry of $\overleftrightarrow{\chi}^{(2)}$ for quartz is also different from that for metal, leading to a different output polarization, even though the output beam direction is still determined by the wavevector component of $\vec{P}^{NL}(2\omega)$ along the surface. As a special case, consider the second harmonic generation by counter-propagating surface plasmons at a quartz-silver interface[18] with the quartz $\hat{a}$-axis oriented along $\hat{x}$ and the $\hat{b}$-axis along $\hat{z}$. The induced nonlinear polarization in quartz is

$$\vec{P}^{NL} = \hat{x}\, \chi_{11}^{(2)} (\mathcal{E}_{1x}^{+}\mathcal{E}_{1x}^{-} - \mathcal{E}_{1z}^{+}\mathcal{E}_{1z}^{-}) e^{2\beta_1 z - i2\omega_1 t} \tag{37}$$

where $\vec{\mathcal{E}}_1^{+}$ and $\vec{\mathcal{E}}_1^{-}$ are the field amplitudes of the forward and backward fundamental waves respectively. Since $\vec{P}^{NL}(\omega)$ along $\hat{x}$ is nonzero, the second harmonic output along the surface normal should be observable. This is indeed the case. Using the experimental setup in Fig. 10 with the counter-propagating beam provided by mirror reflection, Chen et al.[18] observed the second harmonic output along the surface normal. The output beam was highly directional with a beam spread of $\sim$ 1 mrad. The output intensity as a function of the incidence angle of the exciting laser beam is shown in Fig. 11. The observed maximum occurs at the angle where the surface plasmons were optimally excited, and the width of the peak is approximately the width of the surface plasmon resonance observed in the linear reflection curve, similar to the one in Fig. 3. The experimental results were in very good agreement with the theoretical calculation following Sec. II, as shown in Fig. 11. Even the absolute output power agreed well with the prediction of $\mathcal{P}(\omega) = 5 \times 10^{-25} \mathcal{P}^{+}(\omega_1)\, \mathcal{P}^{-}(\omega_1)/A$ in cgs units, where A is the beam overlapping area at the interface.

In Fig. 12, a typical dispersion curve of surface plasmons at a metal-air or metal-dielectric (transparent) interface is shown. It is seen that $|K_x'(\omega = 2\omega_1)| > |2K_x'(\omega_1)|$, and therefore, phase-matched second harmonic generation of surface plasmons by surface plasmons is clearly impossible. In the case of a single exciting laser beam, if the angle of beam incidence is varied to vary k_{1x}, the second harmonic output should exhibit two separate peaks.[7] An example is shown in Fig. 13 for

an aluminum-quartz interface with Nd:YAG laser excitation.[20] The first peak at smaller angle corresponds to the linear excitation of the fundamental surface plasmons, while the second peak arises because of nonlinear excitation of the second harmonic surface plasmons. Since the second harmonic output is proportional to the square of the resonant excitation profile of the fundamental, but only linearly to that of the second harmonic, the first peak is much sharper and stronger than the second one. The difference becomes larger when $K_x'(\omega) - 2K_x'(\omega_1)$ increases. In Fig. 13, the experimental results for the Aℓ-quartz interface are in good accord with the theoretical calculation. Simon et al.[7] first studied second harmonic generation by surface plasmons at a silver-quartz interface. The surface plasmon dispersion between 1.06 μm and 0.53 μm is appreciably stronger in this case, so that $K_x'(\omega) - 2K_x'(\omega_1)$ is larger. Consequently, the second peak is expected to be 5 orders of magnitude lower than the first peak in a similar plot as Fig. 13. Then, because of interference from second harmonic generation in the prism, they were not successful in observing the second peak experimentally. With TE laser excitation, no fundamental surface plasmon can be excited. However, through the nonlinearity of the quartz, the second harmonic surface plasmons can be nonlinearly excited. In this case, only the second peak in Fig. 13 should be observed. This has also been demonstrated experimentally.[20]

Third harmonic generation by surface plasmons at a metal-dielectric interface can also be observed.[19] The discussion closely follows that for second harmonic generation. The effect of resonant excitation of fundamental surface plasmons can again be easily seen.

Experiments of harmonic generation by surface plasmons have so far

been carried out with visible lasers. On the other hand, the same process in the infrared may be more interesting. First, the attenuation constant K_x'' of the surface plasmons is orders of magnitude less in the infrared. Then, the surface plasmon dispersion is also much less in the infrared so that phase-matching of harmonic generation of surface plasmons by surface plasmons ($K_x'(\omega) = 2K_x'(\omega_1)$) can be approximately satisfied. The harmonic output can then be greatly enhanced, with the possibility of efficient generation of a guided infrared surface wave at a new frequency.

V. Surface Coherent AntiStokes Raman Spectroscopy

Third-order nonlinear optical processes with surface plasmons should in general be readily observable, especially if phase-matching can be achieved and the nonlinear susceptibility shows a resonant enhancement. Thus, one expects that coherent antiStokes Raman scattering (CARS) at a metal-dielectric interface can be easily observed if both input and output are surface plasmons.[21] The nonlinearity responsible for the process usually arises from the dielectric medium, and therefore, the resonance enhancement of the nonlinear susceptibility $\overleftrightarrow{\chi}^{(3)}$ is an explicit display of the Raman resonances of the dielectric medium. Physically, surface CARS can also be understood as a two-step process. Two surface plasmon waves at ω_1 and ω_2 with wavevectors $(\vec{k}_1)_{\|} = \vec{K}_{\|}'(\omega_1)$ and $(\vec{k}_2)_{\|} = \vec{K}_{\|}'(\omega_2)$ interact nonlinearly at the interface via the nonlinearity of the medium, where $K_{\|}'(\omega)$ describes the surface plasmon dispersion. They first beat with each other and coherently excite a Raman resonance of the medium at $\omega_1 - \omega_2$ with a wavevector $(\vec{k}_1)_{\|} - (\vec{k}_2)_{\|}$. Then, the ω_1

wave also acts as a probe beam and mixes with the material excitational wave to generate a nonlinear polarization, and hence a coherent output, at $\omega_a = 2\omega_1 - \omega_2$ with a wavevector component along the interface $(\vec{k}_a)_{\parallel} = 2(\vec{k}_1)_{\parallel} - (\vec{k}_2)_{\parallel}$. Clearly, the output should be a maximum when $(\omega_1 - \omega_2)$ is exactly on resonance $(\omega_1 - \omega_2 = \omega_{ex})$, and when $(k_a)_{\parallel} = K'_{\parallel}(\omega_a)$ such that the antiStokes surface plasmons at ω_a are resonantly excited (or in other words, generated under the phase-matching condition).

As in the case of bulk CARS,[22] if the surface plasmon fields are $\vec{E}(\omega_1)$ and $\vec{E}(\omega_2)$, then the nonlinear polarization induced in the dielectric is

$$\vec{P}^{NL}(\omega_a) = \overleftrightarrow{\chi}^{(3)}(\omega_a = 2\omega_1 - \omega_2) : \vec{E}_1(\omega_1)\vec{E}_1(\omega_1)\vec{E}_2^*(\omega_2) \tag{38}$$

where the nonlinear susceptibility can be written as the sum of a resonant part and a nonresonant part

$$\overleftrightarrow{\chi}^{(3)}(\omega_a) = \overleftrightarrow{\chi}_R^{(3)} + \overleftrightarrow{\chi}_{NR}^{(3)}$$

$$\overleftrightarrow{\chi}_R^{(3)} = \frac{\overleftrightarrow{A}}{[(\omega_1 - \omega_2) - \omega_{ex}] + i\Gamma} . \tag{39}$$

With $\vec{P}^{NL}(\omega_a)$ in Eq. (38) as the source term for the coherent output at ω_a, the theory formulated in Sec. II can again be used to describe surface CARS. Since the output is proportional to $|\vec{P}^{NL}(\omega_a)|^2$, and hence $|\chi^{(3)}(\omega_a)|^2$, it should clearly exhibit a resonant enhancement when $(\omega_1 - \omega_2)$ approaches ω_{ex}. The output should also be greatly enhanced if first, the input surface plasmon fields $\vec{E}_1(\omega_1)$ and $\vec{E}_2(\omega_2)$ are enhanced through

resonant excitation (using the Kretschmann geometry), and then the output surface plasmon is also resonantly excited by having $2(\vec{k}_1)_{\|} - (\vec{k}_2)_{\|} \cong \vec{K}'(\omega_a)$. We note that in this case, even though it is a third-order effect, and $\vec{P}^{NL}(\omega_a)$ only exists over a very thin layer at the interface, the output may still be easily detectable simply because $|\vec{P}^{NL}(\omega_a)|$ can be unusually large through the surface plasmon enhancement of the input fields.

Experimental demonstration of surface CARS has been carried out by Chen et al.[21] The setup is shown in Fig. 14. A Q-switched ruby laser pumping a dye laser system was able to deliver two beams at ω_1 and ω_2, each with 20 mJ/pulse and a linewidth ≤ 1 cm^{-1}. The beams excited the surface plasmons through the prism coupler. Their directions could be adjusted to vary $(\vec{k}_1)_{\|}$ and $(\vec{k}_2)_{\|}$ and phase-matched generation of anti-Stokes surface plasmons was possible with $2(\vec{k}_1)_{\|} - (\vec{k}_2)_{\|} \simeq \vec{K}'_{\|}(\omega_a)$ as sketched in Fig. 14(b). Surface CARS and bulk CARS signals were simultaneously monitored. The latter was used for frequency calibration and normalization.

Figure 15 shows the results of antiStokes output versus $(\omega_1 - \omega_2)$ with benzene as the dielectric medium. The resonant peak here corresponds to the 992-cm^{-1} Raman mode of benzene. The peak is slightly asymmetric, indicating that $\chi^{(3)}_{NR}$ is non-negligible. The theoretical curve in Fig. 15 was derived using the known values of $\chi^{(3)}_{NR}$, $\chi^{(3)}_{R}$, ω_{ex}, and Γ in the literatures. It is seen that the agreement between theory and experiment is excellent. That surface CARS can be used as a spectroscopic technique is then obvious. The signal-to-noise ratio detected was very good. At the peak, with 10 mJ/cm^2 pulses of 30-nsec pulsewidth,

the output was 1.5×10^6 photons/pulse, which was also in good agreement with the theoretical estimate. Since in surface CARS, the output is essentially originated from $\vec{P}^{NL}(\omega_a)$ induced by the surface plasmons in a very thin layer (of the order of a reduced wavelength $\lambda/2\pi$) at the interface, the coherent antiStokes signal is not expected to decrease appreciably if instead of a semi-infinite dielectric meidum, a $\sim$ 1000 Å dielectric overlayer on the metal surface is used. Thus, surface CARS should be most useful for Raman spectroscopic study of overlayers.

As we mentioned earlier, the output also depends critically on the resonant excitation of surface plasmons. This was demonstrated experimentally by simply rotating the prism assembly about the $\hat{y}$-axis in Fig. 14 with respect to the incoming beams. The rotation changed $(\vec{k}_1)_{\|}$ and $(\vec{k}_2)_{\|}$, which caused a variation in the resonance conditions of the linear excitation of the surface plasmons at ω_1 and ω_2 and also the nonlinear excitation of the surface plasmons at ω_a. As shown in Fig. 16, the output falls rapidly away from the angular position for optimum excitation of all surface plasmons. The experimental data agreed well with the theoretical calculation. In a separate experiment, the surface plasmons at ω_1 and ω_2 were always being optimally excited, but the phase mismatch $\Delta k_{\|} = |2(\vec{k}_1)_{\|} - (\vec{k}_2)_{\|} - K'_{\|}(\omega_a)|$ for the resonant excitation of the surface plasmons at ω_a was varied. The output versus $\Delta k_{\|}$ showed a Lorentzian line centered at $\Delta k_{\|} = 0$ as expected. Other theoretical predictions for surface CARS were also experimentally verified. For example, the output had a TM polarization characteristic of surface plasmons, and it disappeared with TE excitation. It was also found that the output dependence on the input laser intensities was $I^2(\omega_1)I(\omega_2)$ as predicted.

Aside from the large induced nonlinear polarization and small field penetration depth into the dielectric medium at the interface, surface CARS also has the characteristics of a highly directional output as determined by $(\vec{k}_a)_{\|}$ and a short interaction length. The last aspect results from the high attenuation coefficient $K_{\|}''$ of the surface plasmons in the visible. Typically, the attenuation length is $\ell = 1/K_{\|}'' \sim 10$ μm for surface plasmons at a silver-dielectric interface. The interaction length in surface CARS is therefore only of the order of 10 μm. This strong attenuation is the consequence of the large imaginary part in the metal dielectric constant. The absorption of the dielectric medium will not change $K_{\|}''$ appreciably as long as its corresponding bulk attenuation length is not much shorter than 10 μm. Consequently, the antiStokes output will not be seriously affected by the strong absorption of the dielectric medium. This was actually demonstrated experimentally.[19] The short interaction length together with the highly directional antiStokes output makes surface CARS particularly suitable for spectroscopic study of materials with strong absorption and luminescence. Since the output comes out from the prism side, the luminescence background is further reduced by the shielding of the metal film separating the prism from the dielectric.

It is interesting to estimate the ultimate sensitivity surface CARS can have for detecting molecular overlayers. As we discussed earlier, the output increases with the input laser intensities as $I^2(\omega_1)I(\omega_2)$. It then seems desirable to focus the exciting beams on the surface as tight as possible even though the signal is also inversely proportional to the excitation area. The maximum laser intensity is, however, limited

by the optical damage on the surface. Since the damage usually has a fluence threshold rather than an intensity threshold, the maximum laser intensity can be orders of magnitude higher if picosecond pulses instead of nanosecond pulses are used. Thus, we expect that the ultimate sensitivity of surface CARS can be greatly improved by using picosecond pulse excitation. As an example, we consider surface CARS on a silver-benzene interface. The maximum laser fluence the silver film can withstand is around 25 mJ/cm^2. It is therefore safe to use 10-psec pulses with 10 μJ/pulse focused to a spot of 0.15 mm^2. From the experimental results with Q-switched pulses, the output from surface CARS was estimated to be $S \sim 10^{-23} I\!P^2(\omega_1)\, I\!P(\omega_2) T/A^2$ photons/pulse, where the input powers $I\!P(\omega_1)$ and $I\!P(\omega_2)$ are in ergs/sec, T is the pulsewidth in sec, and A is the beam overlapping in cm^2. Then, with the 10-psec pulses, the output signal can be $\sim 10^{11}$ photons/pulse. Reduction of the pulsewidth to 1 psec with the input pulse energy kept unchanged will increase the signal by another two orders of magnitude. We recall that in surface CARS, the signal mainly comes from the nonlinearly induced oscillating dipoles in a surface layer of $\sim \lambda/2\pi$ thick that contains several hundred atomic or molecular layers. If we now have only a single monolayer of molecules on silver, the antiStokes output, being coherent, is proportional to the square of the number of molecules radiating, and therefore, should decrease by a factor of $10^4 - 10^5$. Even so, the signal is still as large as $10^6 - 10^7$ photons/pulse and should be easily detected. Thus, we conclude that surface CARS should have an ultimate sensitivity of being able to detect submonolayers of molecules on metals.

VI. Concluding Remarks

We have seen in this chapter various different cases of nonlinear wave interaction involving surface polaritons: generation of surface polaritons by mixing of bulk waves and by mixing of bulk and surface waves, generation of bulk waves by mixing of surface polaritons and by mixing of bulk and surface waves, and wave mixing with all input and output waves being surface polaritons. As presented in Sec. II, they can be described by the same general theoretical formalism. Second-order nonlinear optical processes with surface polaritons are strong only if one or both media at the interface lack inversion symmetry. If both media have inversion symmetry, the processes become much weaker. However, they may be more interesting from the surface physics point of view, since in such cases, the nonlinearity may be dominated by the few atomic or molecular layers at the interface. Then, the second-order effects may be used as probes to study the physical properties of these surface layers.

The third-order nonlinear processes involving surface polaritons are generally weaker than the second-order processes. They can, however, become fairly strong when the relevant nonlinear susceptibility undergoes a resonant enhancement. Thus, with picosecond excitation pulses, surface CARS can have a sensitivity of detecting a submonolayer of molecules adsorbed to the surface, and may become a very useful technique for spectroscopic study of adsorbed molecules. The latter is an important problem in surface physics. Electron loss spectroscopy is at present commonly used for measurements of vibrational spectra of adsorbed molecules. It has only a resolution of $\sim 100\ cm^{-1}$, and is not capable of detecting

small shifts in the vibrational frequencies due to weak bonding in adsorption. Surface CARS can have a resolution better than 1 cm^{-1}, and therefore should yield more valuable information than electron loss spectroscopy. In addition, with picosecond excitation pulses, dynamic behavior or adsorbed molecules can also be studied down to the picosecond time regime. Applications to the detailed studies of adsorption process, molecular reaction, catalytical action, etc. should certainly be considered.

Resonant surface CARS is another interesting area that is yet to be investigated. The additional electronic resonance of the medium seen by either or both input waves should further enhance the output signal, and allow the process to be more selective in specifying the molecules or vibrational modes. This is quite similar to resonant Raman scattering. The resonant surface CARS is particularly attractive in view of the fact that surface CARS is most suited for study of materials with strong absorption and luminescence. CARS is, of course, only a special case of the general four-wave mixing processes. In general, surface four-wave mixing with resonant excitation of materials should also be observable, and can be used for spectroscopic study. For example, two-photon absorption spectra of molecular layers can certainly be obtained by surface four-wave mixing.

Aside from optical mixing, other nonlinear optical effects involving surface polaritons should, in principle, also exist. Stimulated Raman scattering, for example, is one such effect that should be readily observable. In fact, Heritage[23] has recently reported the observation of stimulated Raman gain from a monolayer of molecules using bulk waves. If surface plasmons are used in the same experiment, the beam intensities

at the molecules will be greatly enhanced, and the Raman gain can therefore be orders of magnitude higher. The Raman gain spectroscopy is another potentially useful method for study of submonolayer of molecules on surfaces.

The Kretschmann geometry for linear excitation of surface plasmons may be most convenient for study of metal-dielectric interfaces, if crystalline metal is not required. For other interfaces, however, the Otto geometry may be more suitable. Technical difficulties still exist in the excitation of surface polaritons, especially when high coupling efficiency is needed, as in the case of study of nonlinear interaction of surface polaritons. These difficulties can hopefully be overcome if more effort is devoted to the research of surface polaritons.

Acknowledgement: This work was supported by the Division of Materials Sciences, Office of Basic Energy Sciences, U. S. Department of Energy, under contract No. W-7405-ENG-48.

References

1. See, for example, G. Borstel and H. J. Falge, Applied Physics 16, 211 (1978) and references therein.
2. F. DeMartini and Y. R. Shen, Phys. Rev. Lett. 36, 216 (1976).
3. N. Bloembergen and P. S. Pershan, Phys. Rev. 128, 606 (1962).
4. F. DeMartini, G. Giuliani, P. Mataloni, E. Palange, and Y. R. Shen, Phys. Rev. Lett. 37, 440 (1976).
5. F. DeMartini, M. Colocci, S. E. Kohn, and Y. R. Shen, Phys. Rev. Lett. 38, 1223 (1977).
6. H. J. Simon, D. E. Mitchell, and J. G. Watson, Phys. Rev. Lett. 33, 1531 (1974).
7. H. J. Simon, R. E. Benner, and J. G. Rako, Optics Comm. 23, 245 (1977).
8. N. Bloembergen, R. K. Chang, S. S. Jha, and C. H. Lee, Phys. Rev. 174, 813 (1968).
9. C. K. Chen, A. R. B. de Castro, Y. R. Shen, and F. DeMartini, Phys. Rev. Lett. 43, 946 (1979).
10. A. Sommerfeld, Ann. Physik 28, 665 (1909).
11. See, for example, M. Born and E. Wolf, Principles of Optics, 3rd Ed. (Pergamon Press, New York, 1965) p. 61.
12. A. Otto, Z. Phys. 216, 398 (1968).
13. E. Kretschmann, Z. Phys. 241, 313 (1971).
14. N. Marschall and B. Fischer, Phys. Rev. Lett. 28, 892 (1972).
15. A. S. Barker, Phys. Rev. 165, 917 (1968).
16. J. Lagois and B. Fischer, Phys. Rev. Lett. 36, 680 (1976).

17. See, for example, A. Hartstein, E. Burstein, J. J. Brion, and R. F. Wallis, Solid State Comm. 12, 1083 (1973).

18. C. K. Chen, A. R. B. de Castro, and Y. R. Shen, Optics Lett. 4, 393 (1979).

19. C. K. Chen and A. R. B. de Castro, private communications.

20. F. DeMartini, P. Ristori, E. Santamato, and A. C. A. Zammit, to be published.

21. C. K. Chen, A. R. B. de Castro, and Y. R. Shen, Phys. Rev. Lett. 43, 946 (1979).

22. See, for example, M. D. Levenson, Physics Today 30, 45 (1977).

23. J. P. Heritage, Topical Meeting on Picosecond Phenomena, Cape Cod, Mass., June 18, 1980, paper FA 8.

Figure Captions

Fig. 1 Electromagnetic wave propagation in a layered medium. Incident wave from $z < z_o$ propagates along $+\hat{z}$.

Fig. 2 (a) Otto configuration and (b) Kretschmann configuration for linear excitation of surface polaritons.

Fig. 3 An example of reflectivity versus incidence angle in the Kretschmann configuration. Here, the sharp dip indicates the resonant excitation of surface plasmons at the silver-liquid crystal interface (after Fig. 2(c) of K. C. Chu, C. K. Chen, and Y. R. Shen, Mol. Cryst. Liq. Cryst. 59, 97 (1980)).

Fig. 4 Dispersion characteristics of surface polaritons at the air-GaP interface. (a) K_x' versus ω, and (b) K_x'' versus ω. The solid curves are calculated from the single oscillator model using Eqs. (24) and (25). The dashed curves are calculated from the multi-oscillator model of Ref. 15.

Fig. 5 Experimental setup for nonlinear optical excitation and detection of surface polaritons. The inset shows the wavevector relation for the nonlinear mixing process.

Fig. 6 Examples of experimental data on $I(\omega_4,\Delta k_x)$ versus Δk_x in the GaP case. The solid curves are Lorentzian used to fit the data.

Fig. 7 Experimental setup for observing second harmonic generation of surface exciton-polariton on ZnO. The inset shows the wavevector relation.

Fig. 8 Examples of experimental results of $I(\omega,\Delta k_x)$ versus Δk_x in the ZnO case. The solid cruves are Lorentzian used to fit the data.

Fig. 9 Dispersion and damping characteristics of surface exciton-polaritons on ZnO. The solid curves are theoretical curves calculated from Eqs. (30) and (31).

Fig. 10 Experimental setup for observing second harmonic generation by counter-propagating surface plasmons.

Fig. 11 Second harmonic intensity versus the incidence angle θ (defined in Fig. 10).

Fig. 12 A typical dispersion curve of surface plasmons.

Fig. 13 Second harmonic output at the quartz-aluminum interface as a function of the incidence angle, exhibiting two separate peaks.

Fig. 14 Experimental setup for surface CARS measurements. (a) the prism-metal-liquid assembly; (b) wavevectors in the glass prism with their components in the x-y plane phase matched; (c) block diagram of the experimental arrangement.

Fig. 15 AntiStokes output versus $\omega_1 - \omega_2$ around the 992 cm^{-1} Raman resonance of benzene. The solid curve is a theoretical curve.

Fig. 16 AntiStokes signal versus the angular position of the prism assembly about the $\hat{y}$ axis (Fig. 14). θ is the angle between beam 1 and the prism normal.

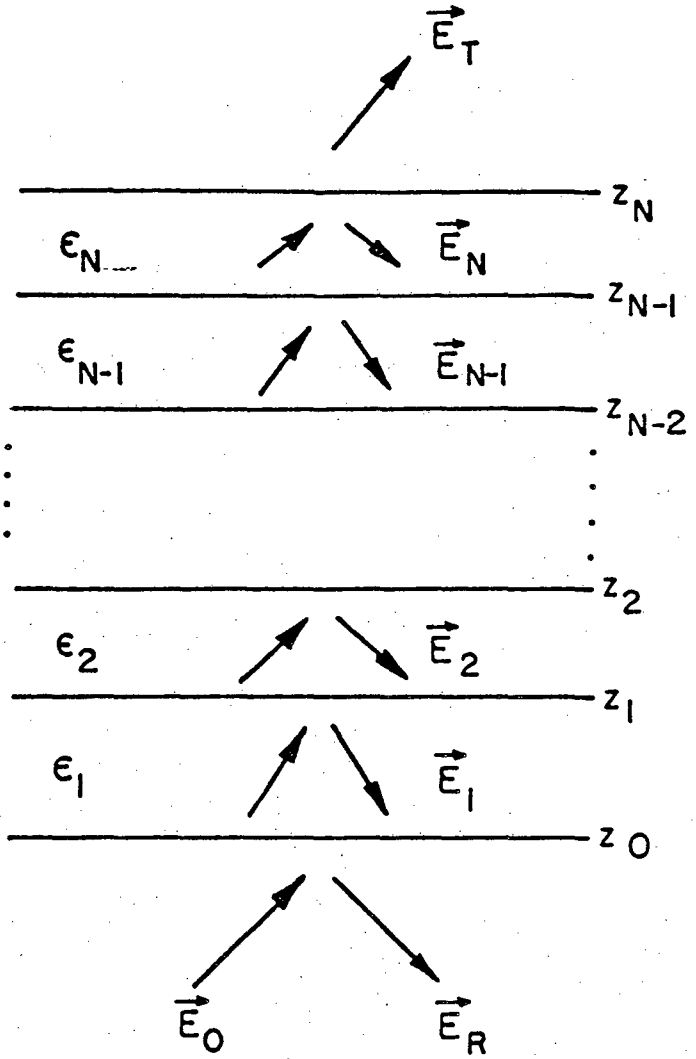
$\vec{E}_T$
z_N
ϵ_N
$\vec{E}_N$
z_{N-1}
ϵ_{N-1}
$\vec{E}_{N-1}$
z_{N-2}
z_2
ϵ_2
$\vec{E}_2$
z_1
ϵ_1
$\vec{E}_1$
z_0
$\vec{E}_0$
$\vec{E}_R$

XBL 808-5759

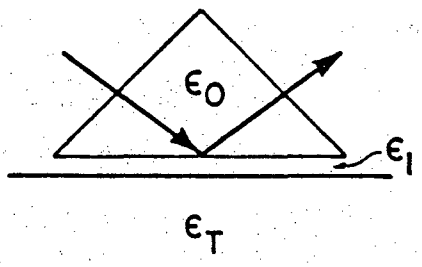

(a)

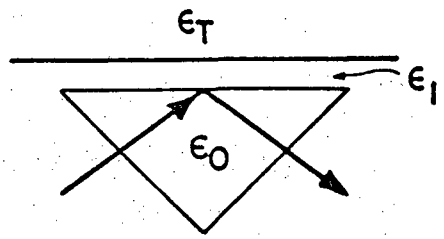

(b)

XBL 808-5760

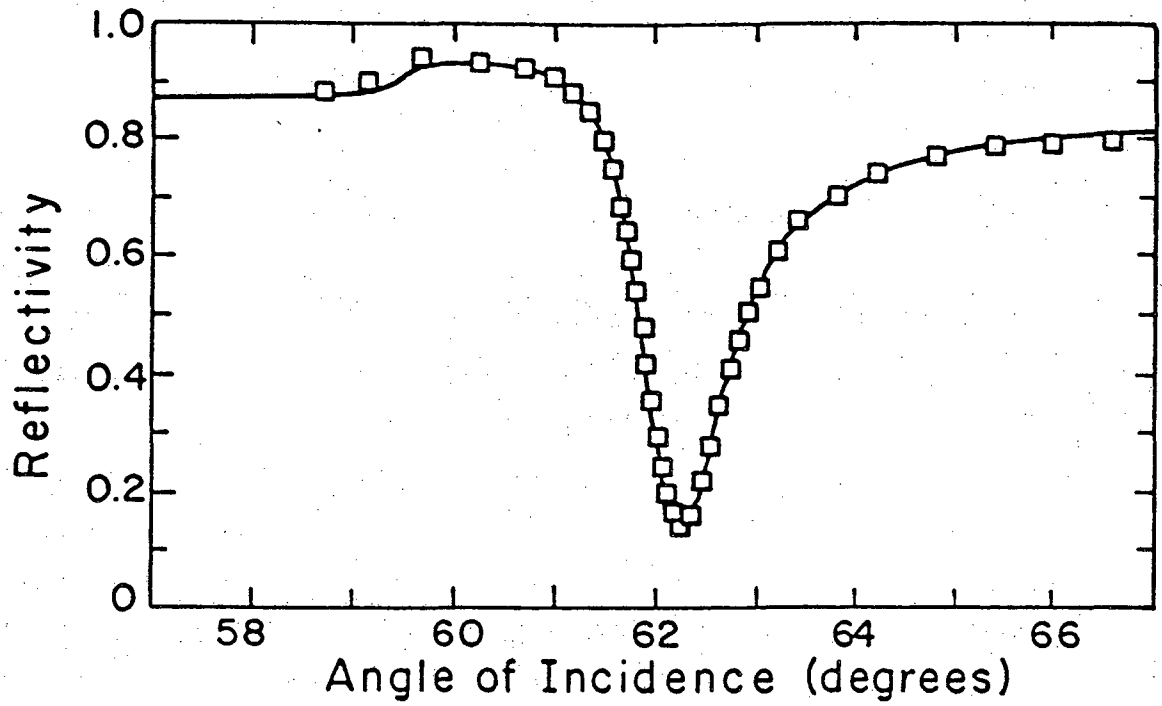

XBL 807-10717

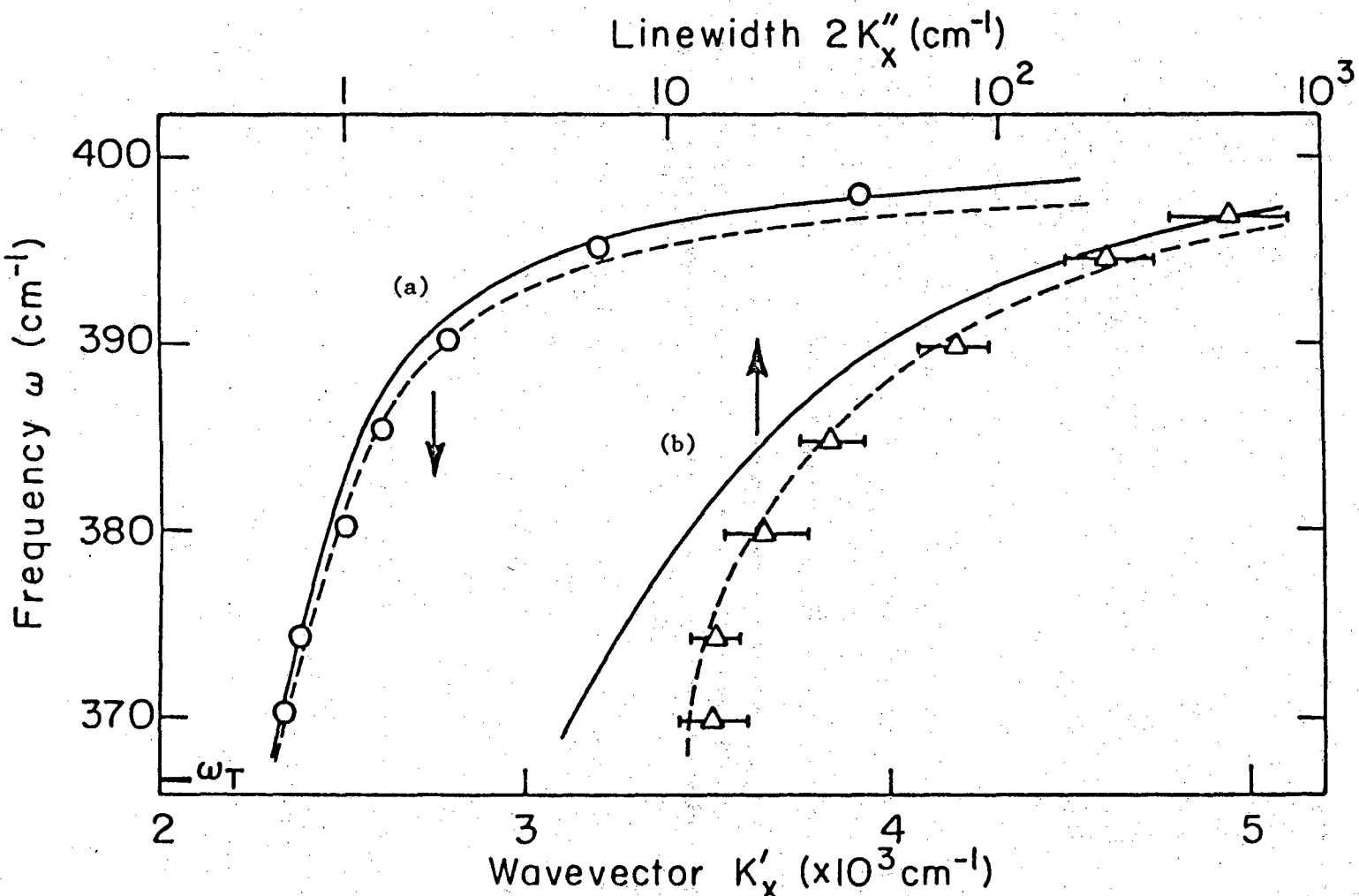
Linewidth $2K_x''$ (cm^{-1})
1
10
10^2
10^3
400
390
380
370
Frequency ω (cm^{-1})
(a)
(b)
ω_T
2
3
4
5
Wavevector K_x' ($\times 10^3 cm^{-1}$)

XBL809-5948

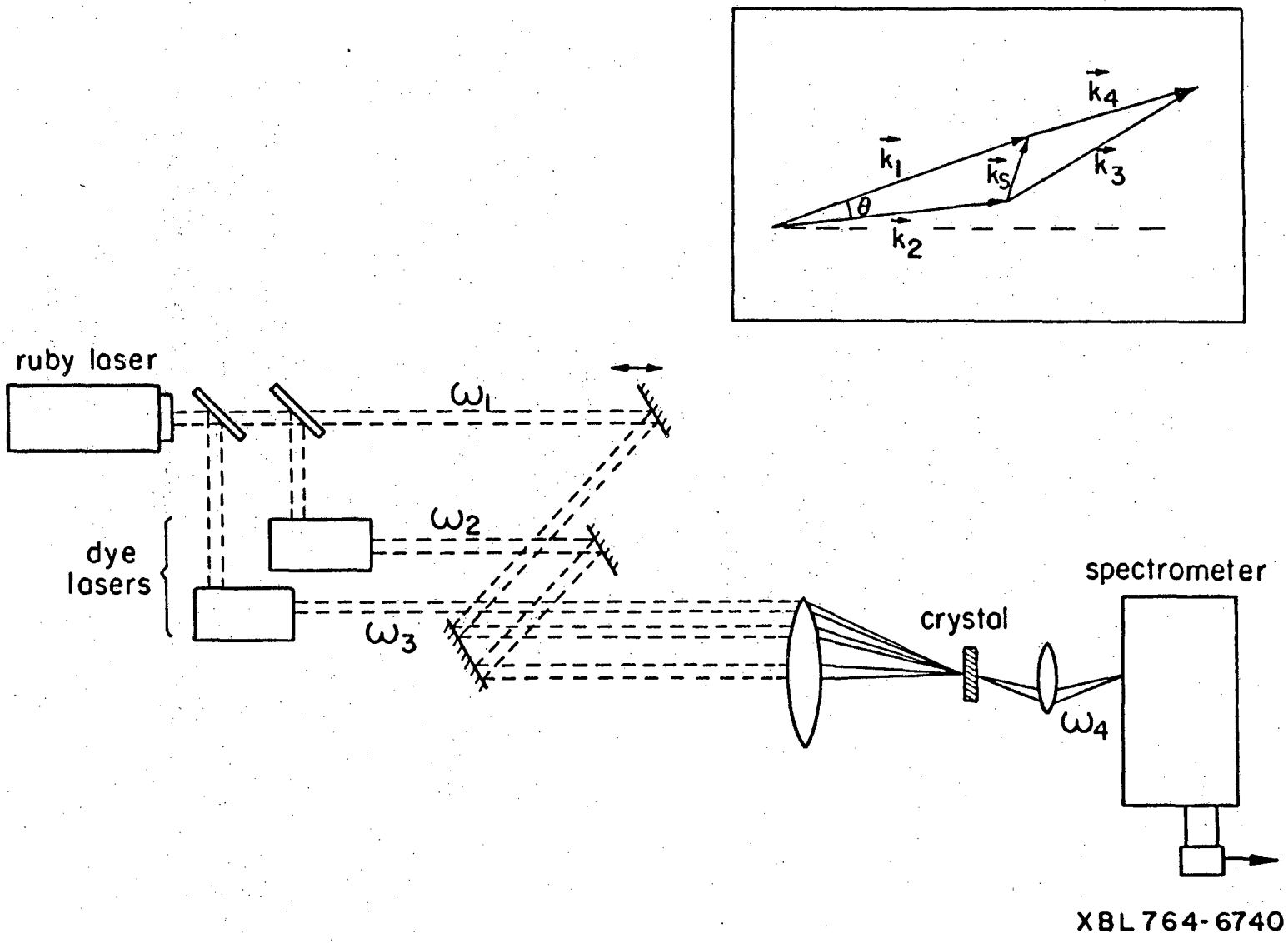
$\vec{k}_4$
$\vec{k}_1$
$\vec{k}_s$
$\vec{k}_3$
θ
$\vec{k}_2$
ruby laser
ω_L
ω_2
dye
lasers
ω_3
spectrometer
crystal
ω_4
XBL764-6740

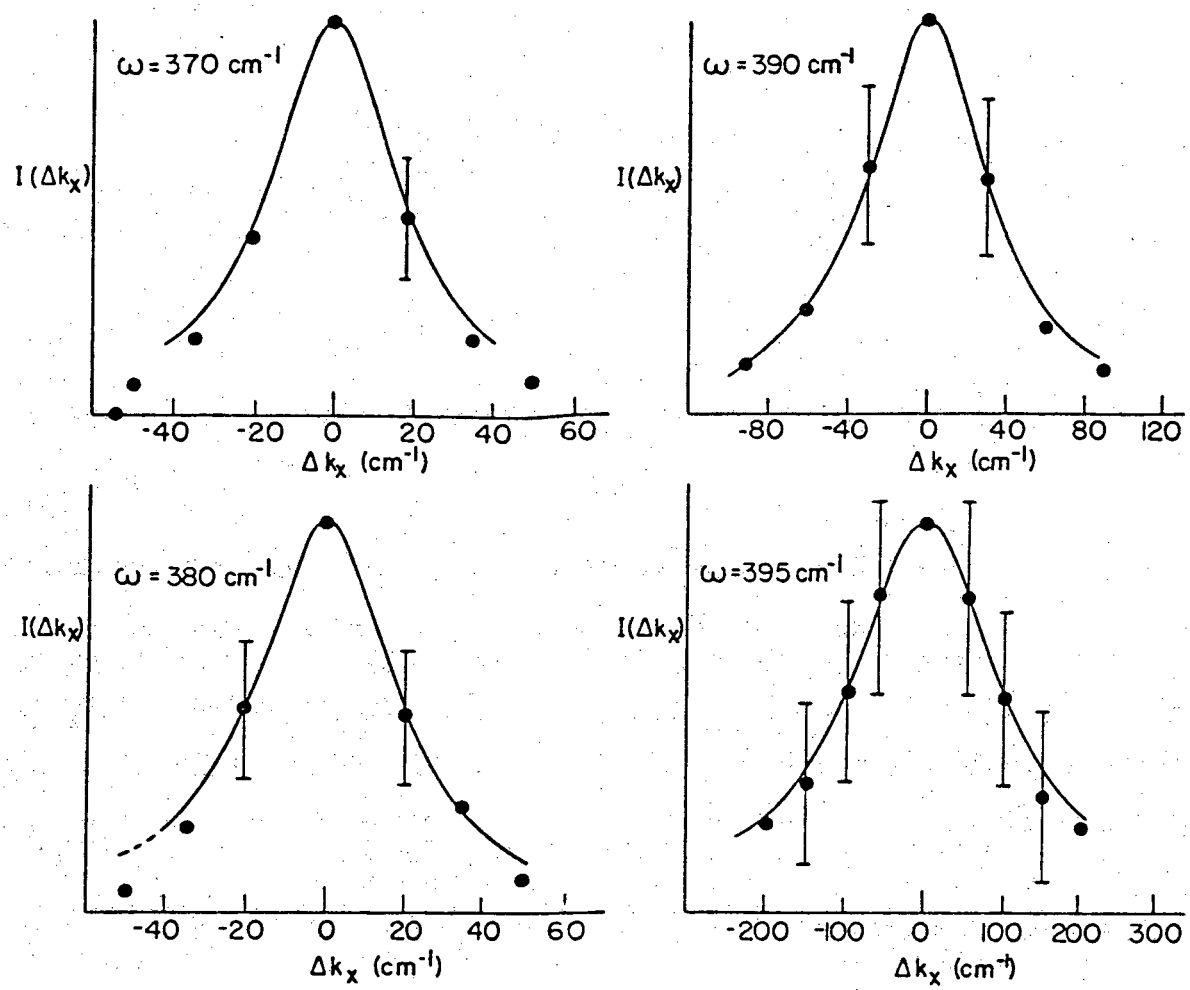
ω = 370 cm⁻¹
I (Δk_x)
-40 -20 0 20 40 60
Δ k_x (cm⁻¹)
ω = 390 cm⁻¹
I(Δk_x)
-80 -40 0 40 80 120
Δ k_x (cm⁻¹)
ω = 380 cm⁻¹
I(Δk_x)
-40 -20 0 20 40 60
Δk_x (cm⁻¹)
ω = 395 cm⁻¹
I(Δk_x)
-200 -100 0 100 200 300
Δk_x (cm⁻¹)

XBL764-6741

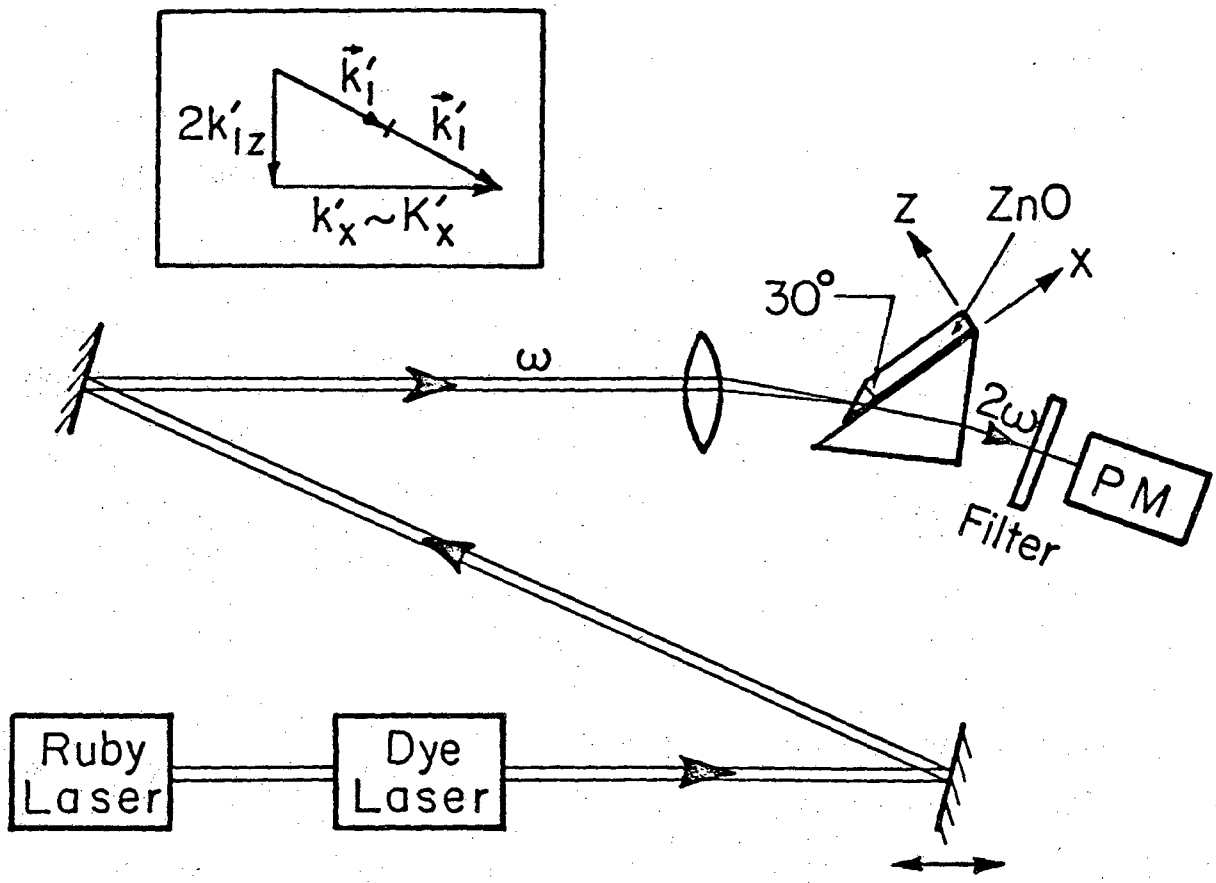
$\vec{k}'_1$
$2k'_{1z}$
$\vec{k}'_1$
$k'_x \sim K'_x$
Z
ZnO
X
30°
ω
2ω
PM
Filter
Ruby Laser
Dye Laser

XBL 772-5095

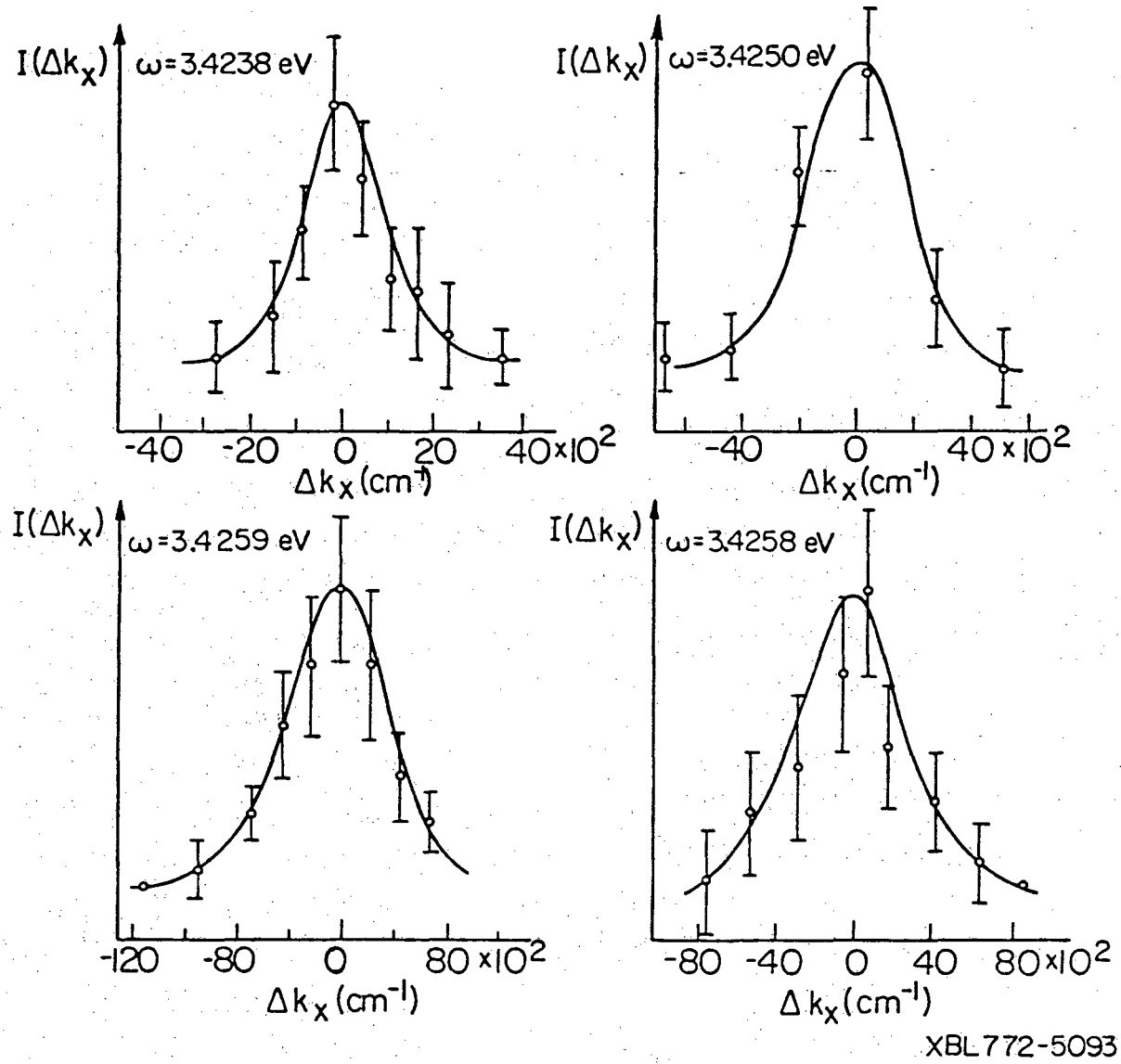
I(Δk_x)
ω=3.4238 eV
-40 -20 0 20 40×10^2
Δk_x (cm^-1)
I(Δk_x)
ω=3.4250 eV
-40 0 40×10^2
Δk_x (cm^-1)
I(Δk_x)
ω=3.4259 eV
-120 -80 0 80×10^2
Δk_x (cm^-1)
I(Δk_x)
ω=3.4258 eV
-80 -40 0 40 80×10^2
Δk_x (cm^-1)

XBL772-5093

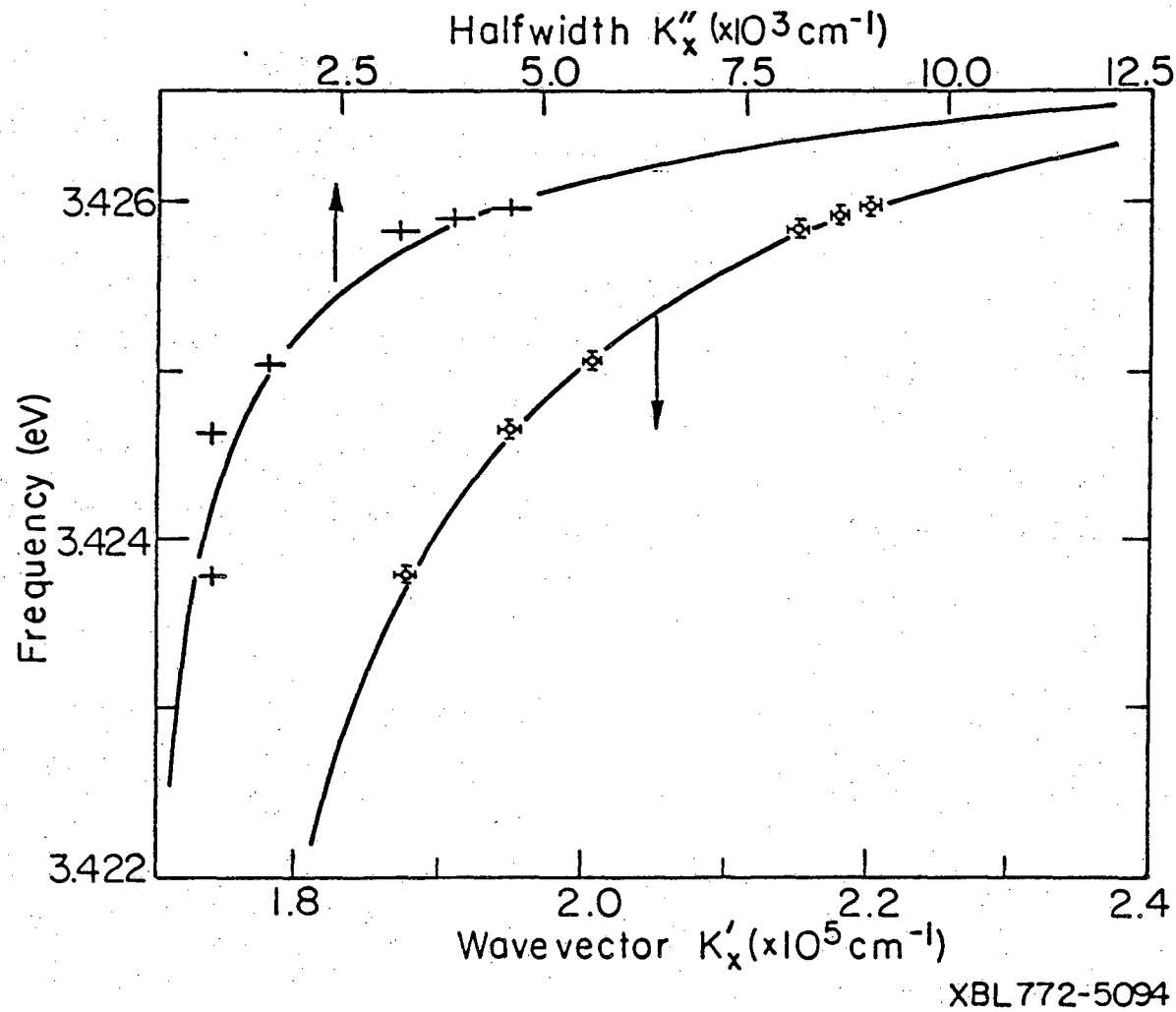
Halfwidth K_x'' (x10^3 cm^{-1})
2.5
5.0
7.5
10.0
12.5
3.426
3.424
3.422
Frequency (eV)
1.8
2.0
2.2
2.4
Wavevector K_x' (x10^5 cm^{-1})

XBL772-5094

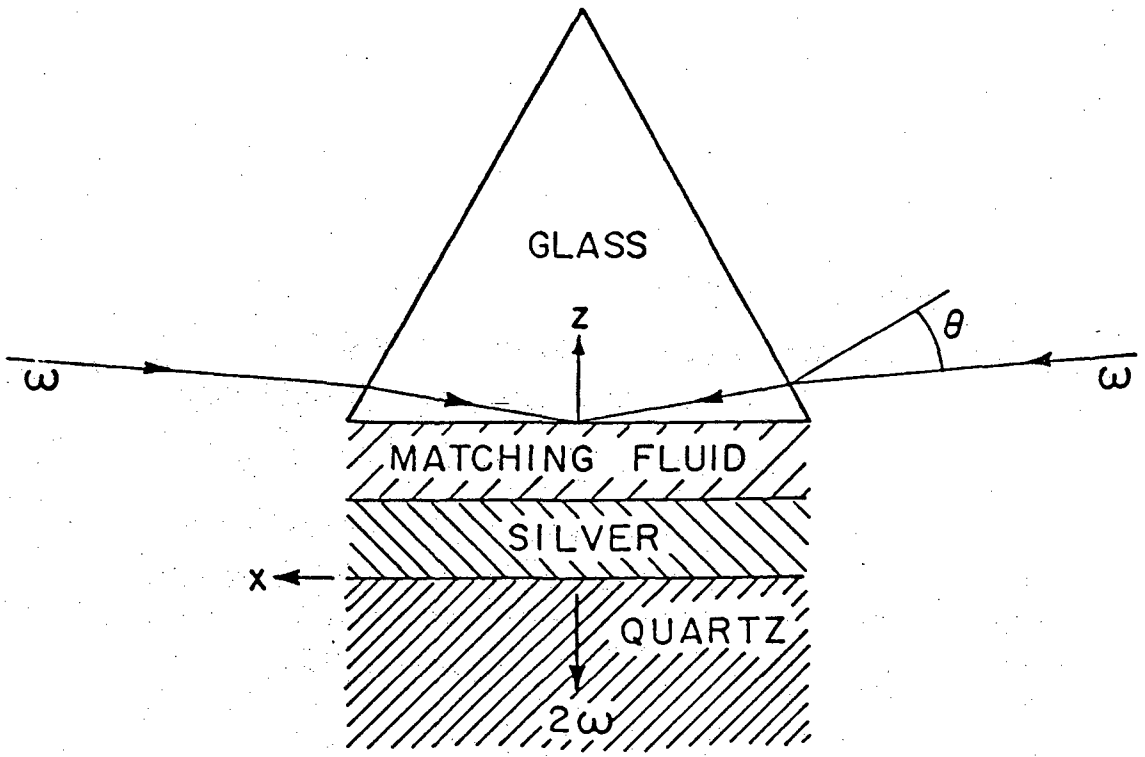

(a)

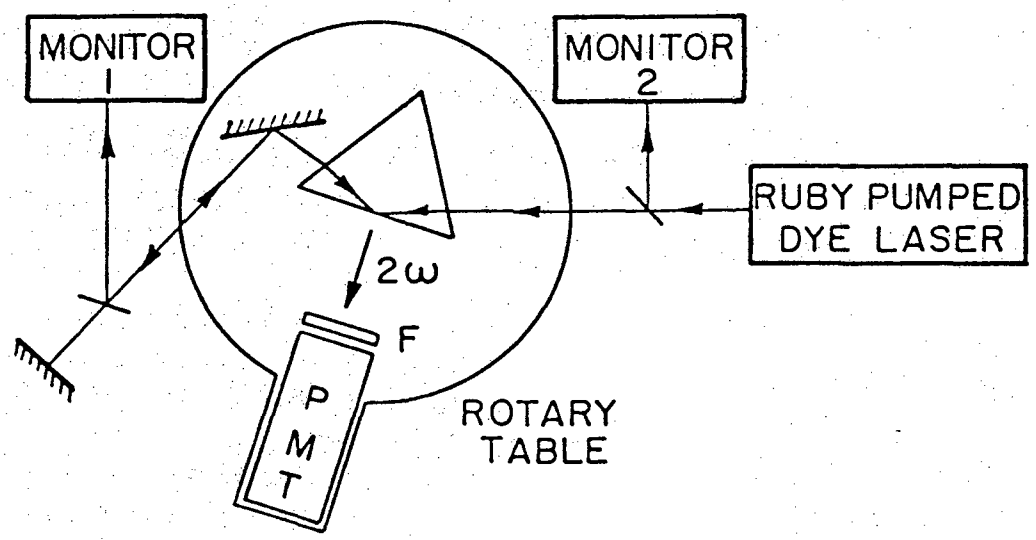

(b)

XBL797-6702

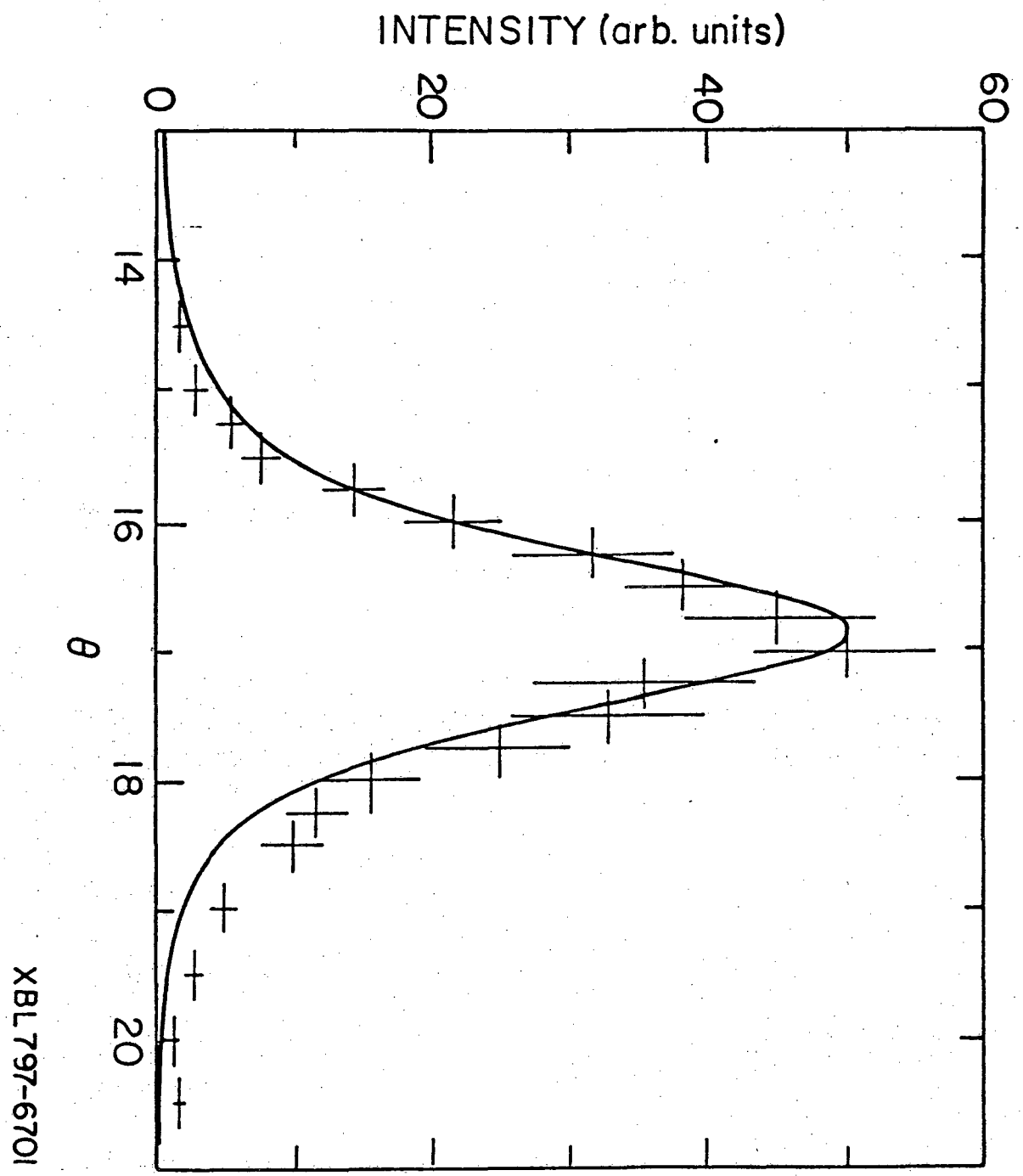
INTENSITY (arb. units)
0
20
40
60
θ
14
16
18
20
XBL797-6701

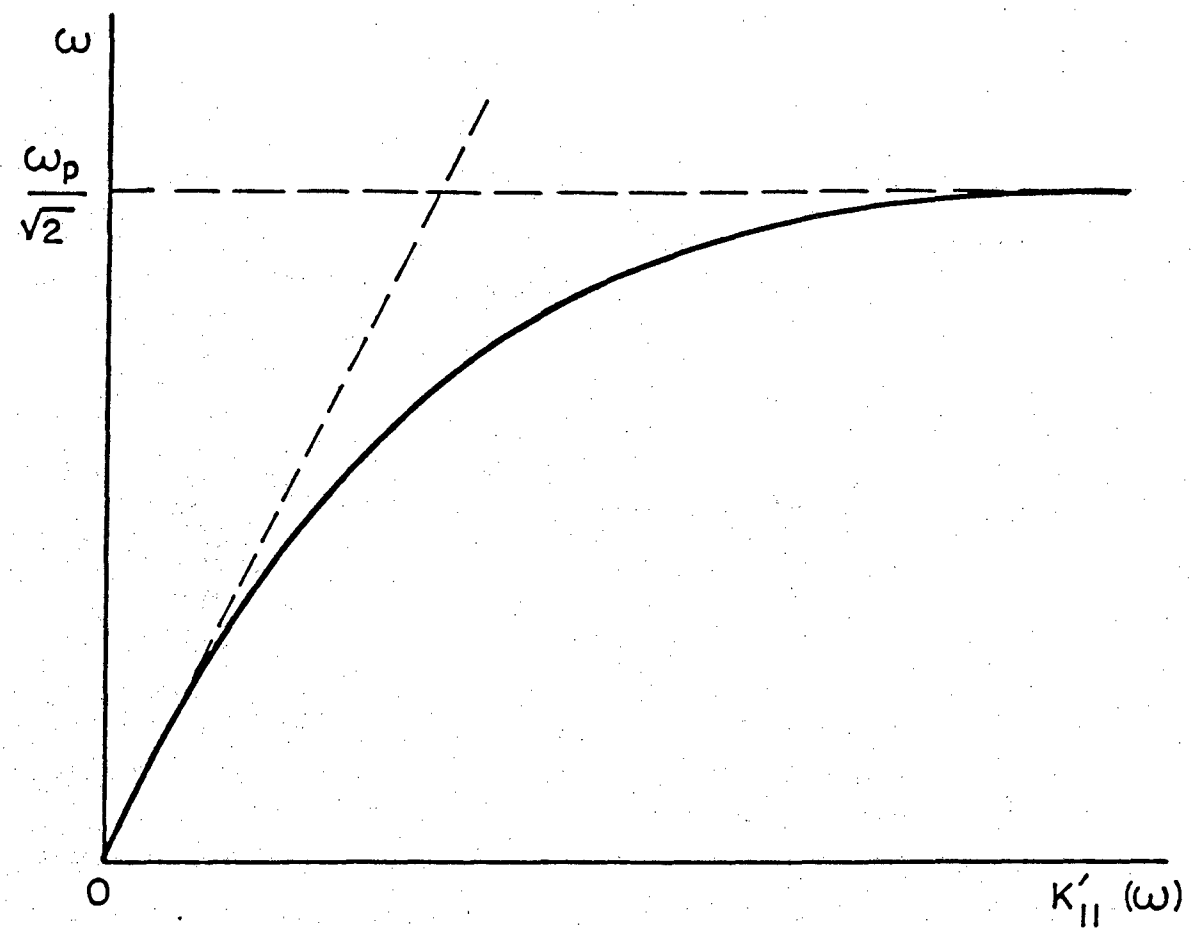

XBL808-5761

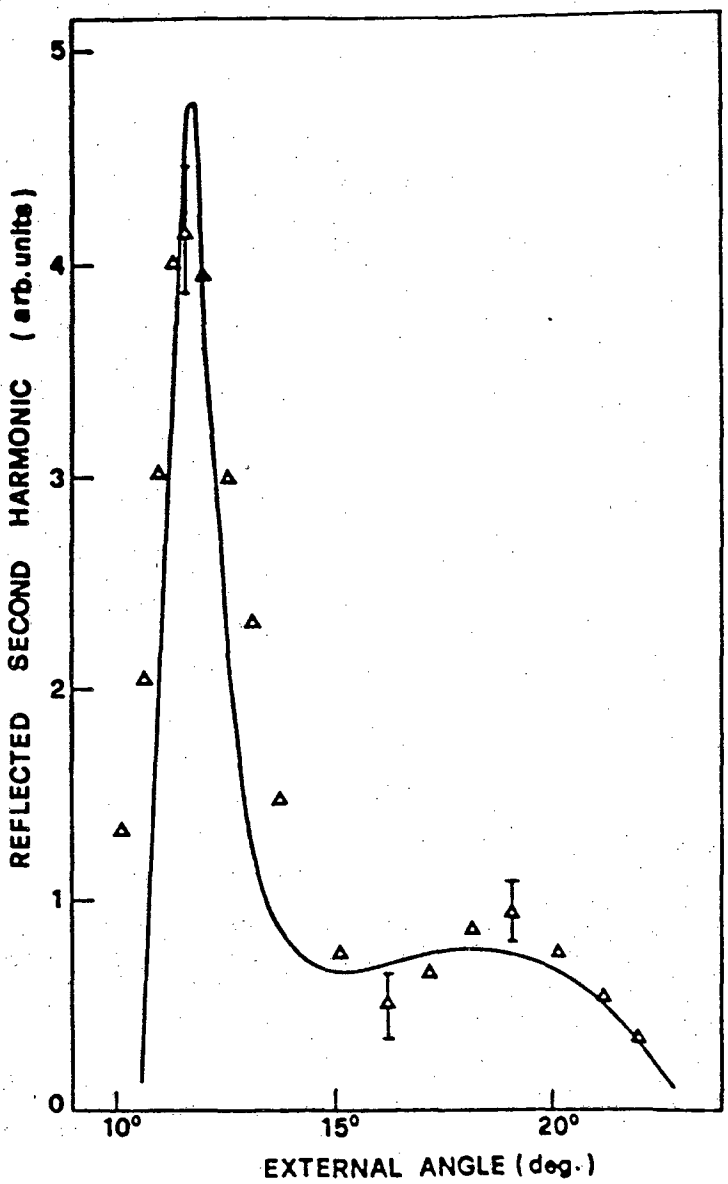

XBL 8010-12262

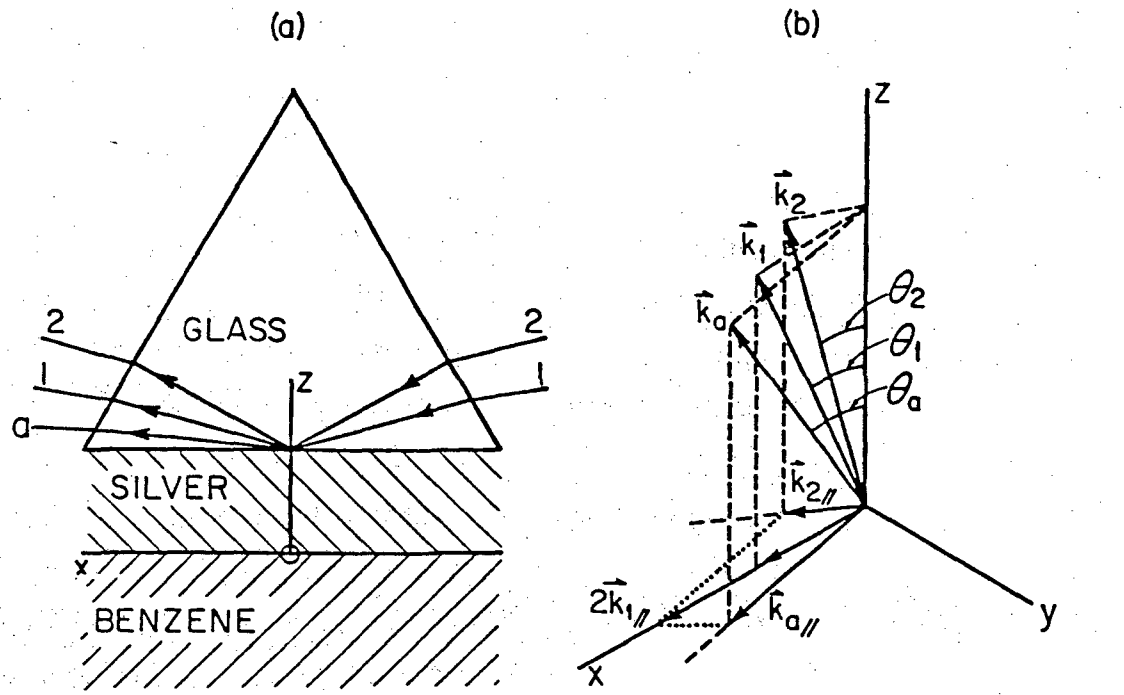

(c)

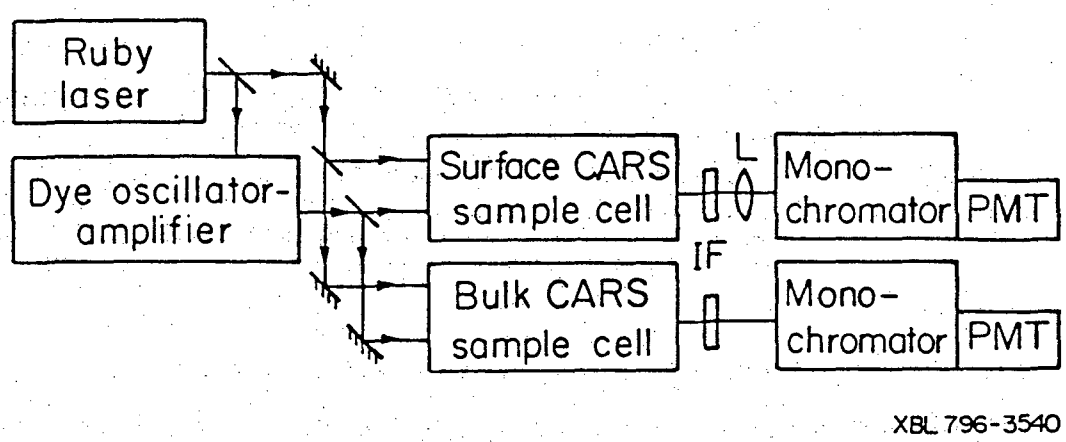

XBL 796-3540

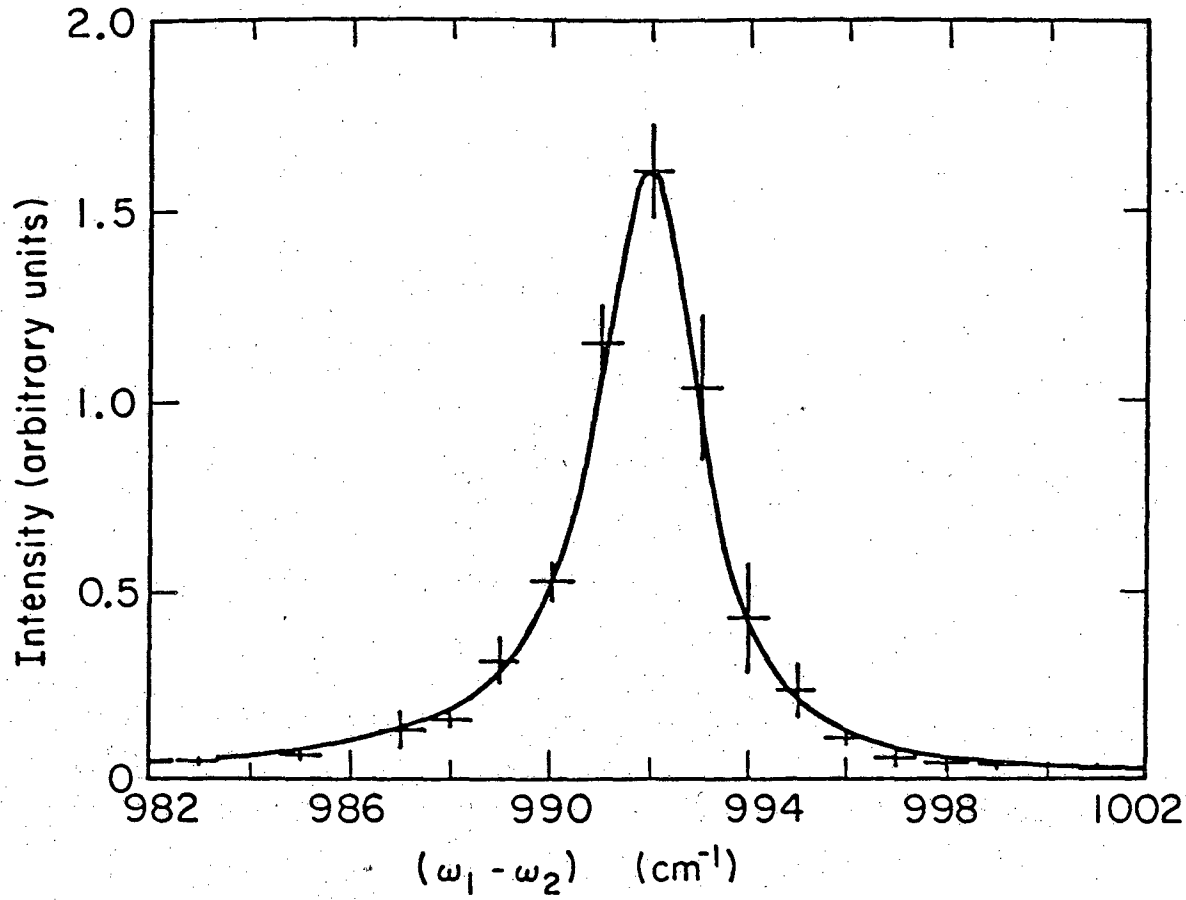
2.0
1.5
1.0
0.5
0
Intensity (arbitrary units)
982
986
990
994
998
1002
(ω1 - ω2) (cm-1)

XBL796-3537

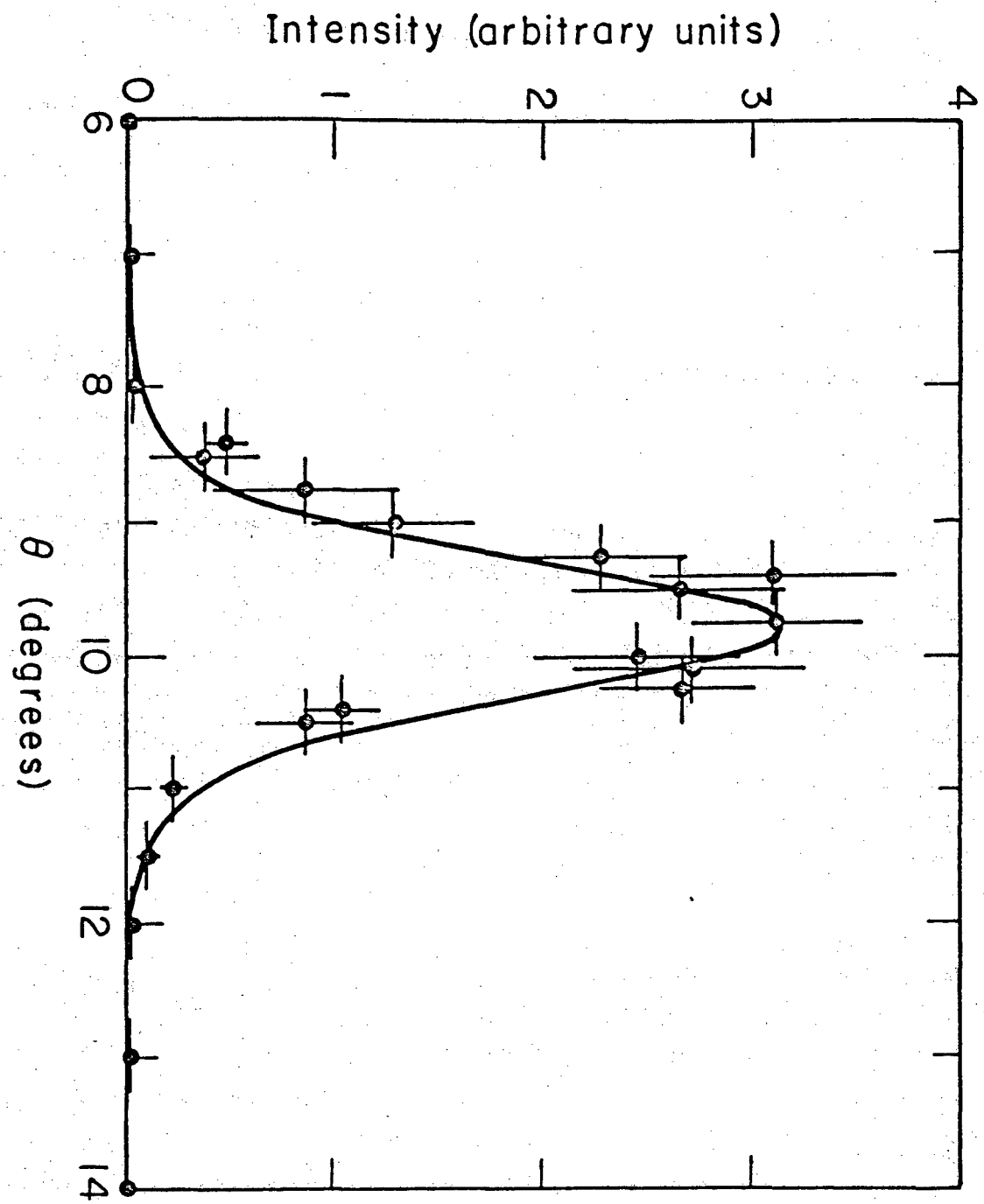

XBL796-3539

This report was done with support from the Department of Energy. Any conclusions or opinions expressed in this report represent solely those of the author(s) and not necessarily those of The Regents of the University of California, the Lawrence Berkeley Laboratory or the Department of Energy.

Reference to a company or product name does not imply approval or recommendation of the product by the University of California or the U.S. Department of Energy to the exclusion of others that may be suitable.

TECHNICAL INFORMATION DEPARTMENT
LAWRENCE BERKELEY LABORATORY
UNIVERSITY OF CALIFORNIA
BERKELEY, CALIFORNIA 94720